

NOAA Technical Memorandum ERL GLERL-18

PHOTOSYNTHETICALLY ACTIVE RADIATION TRANSMITTANCE THROUGH ICE

S. J. Bolsenga

Great Lakes Environmental Research Laboratory  
Ann Arbor, Michigan  
July 1978



UNITED STATES  
DEPARTMENT OF COMMERCE  
Juanita M. **Kreps**, Secretary

NATIONAL OCEANIC AND  
ATMOSPHERIC ADMINISTRATION  
Richard A. Frank, Administrator

Environmental Research  
Laboratories  
Wilmot N. Hess, Director

#### NOTICE

The NOAA Environmental Research Laboratories do not approve, recommend, or endorse any proprietary product **or** proprietary material mentioned in this publication. No reference shall be made to the NOAA Environmental Research Laboratories, or to this publication furnished by the NOAA Environmental Research Laboratories, in any advertising or sales promotion which would indicate or imply that the NOAA Environmental Research Laboratories approve, recommend, **or** endorse any proprietary product **or** proprietary material mentioned herein, or which has as its purpose **an** intent to cause directly or indirectly the advertised product to be used or purchased because of this NOAA Environmental Research Laboratories publication.

## CONTENTS

	Page
Abstract	1
1. INTRODUCTION	2
2. INSTRUMENTATION AND TEST PLAN	7
3. DATA REDUCTION	14
4. ANALYSIS	15
4.1 General	15
4.2 Daily Trends	19
4.3 Snowmobile Disturbances	29
4.4 Diffuse Extinction Coefficients	33
4.5 Reflectance-Transmittance Model	36
4.6 Depth Profiles	39
5. SUMMARY AND CONCLUSIONS	43
6. ACKNOWLEDGMENTS	44
7. REFERENCES	45
Appendix. THE TWO-LAYER MODEL	47

## FIGURES

	Page
1. Incident radiation sensor equipped with leveling unit.	8
2. Underwater sensor assembly details.	9
3. Relative spectral response of the two sensors used in this study.	8
4. Cosine response of typical underwater sensor.	10
5. Design details of the support arm for the underwater sensor.	11
6. <b>Microammeter</b> used for sensor readout and associated deck-to-sea switch.	12
7. Overall and closeup views of drilling operations with barrel shield.	13
8. Progressive clearing of a measurement site to obtain the ratios shown in Figure 9.	16
9. Ratio of under-ice to above-ice radiation (T) versus true solar time (TST) <b>as the ice surface was progressively</b> cleared of a thin snow layer, 26 January 1977.	19
10. A series of measurements showing the contrast between radiation transmittance (T) <b>as a function of true solar time (TST) through ice alone and through the same ice cover with a snow layer,</b> 22 December 1976.	20
11. Sensor and horizontal portion of boom as seen through the clear ice surface on 22 December 1976.	20
12. Ratio of below- to above-ice radiation (T) as a function of true solar time (TST) during a period of melting <b>snow</b> for 7 March 1977.	21
13. Radiation transmittance (T) as a function of true solar time (TST) during ice decay for 8 March 1977.	21
14. Radiation transmittance (T) as a function of true solar time (TST) during ice decay for 9 March 1977.	21

	Page
15. Radiation transmittance (T) versus true solar time (TST) during a period of variable <b>cumulus</b> cloud coverage and during periods between depth profiles for 7 January 1977.	23
16. Ratio of under-ice to incident radiation (T) versus true solar time (TST) for <b>a clear</b> ice surface showing a marked difference between this diurnal pattern and the one observed for refrozen slush, 17 January 1977.	23
17. Increase in radiation transmittance due to <b>snowmelt</b> as indicated by the rise in transmittance ratio (T) with true solar time (TST), 22 February 1977.	25
18. Ratio of under-ice to incident radiation (T) <del>versus</del> true solar time (TST) on a partly cloudy day with a changing ice surface, 6 January 1977.	25
19. Highly variable surface characteristics of refrozen slush. The two surfaces are at different locations from the same borehole.	26
20. Transmittance (T) <b>versus</b> true solar time (TST) showing differences in (T) due to cloud-cover variability for 18 January 1977.	27
21. Transmittance (T) versus true solar time (TST) showing the lack of variability of the ratios due to lack of cloud cover variability, 19 January 1977.	27
22. Ice conditions at the second brash ice site showing snow trapped between the individual blocks of ice.	29
23. Surface conditions at site used to measure radiation transmittance through a natural ice and snow surface and the same surface disturbed by a snowmobile.	30
24. Conditions at the site shown in Figure 23 after irrigation.	30
25. Surface conditions at snowmobile track measurement site showing the undisturbed and disturbed areas and a closeup of the track imprint.	31
26. Overall and detailed views of snowmobile track measurement site.	32

	Page
27. Upper layer reflectance, $p(A)$ , versus combined transmittance, $\tau(C)$ , and upper layer reflectance, $\rho(A)$ , versus combined reflectance, $p(C)$ , from operation of the two-layer model for a situation where the underlying layer simulates clear ice.	37
28. Upper layer reflectance, $p(A)$ , versus combined transmittance, $\tau(C)$ , and upper layer reflectance, $p(A)$ , versus combined reflectance, $p(C)$ , from operation of the two-layer model for a situation where the underlying layer simulates snow ice.	38
29. Radiation transmittance as related to depth for 14, 17, and 22 February 1977.	40
30. Radiation transmittance as related to depth for 7, 8, and 9 March 1977.	41

#### APPENDIX FIGURE

A.1. Schematic Representation of Two-Layer Model.	47
---	----

## TABLES

	Page
1. Transmittance of Radiation Through Ice and Snow.	4
2. Diffuse Extinction Coefficients for Ice and Snow in the 400-700 nm Range.	6
3. Dates, Locations, and Surface Conditions of the Measurement Sites.	15
4. Diffuse Extinction Coefficients Obtained for Selected Situations in this Study and Coefficients Obtained by <b>Maguire (1975b)</b> for the Same Spectral Range.	33
5. Atmospheric Conditions, Solar Altitudes, and Ice Types During Depth Profiles.	42

PHOTOSYNTHETICALLY ACTIVE

RADIATION TRANSMITTANCE THROUGH ICE\*

S. J. Bolsenga

Radiation transmittance through clear, refrozen slush, and brash ice, from the ice surface to the ice-water interface, in the 400-700 nm range varied according to ice type, atmospheric conditions, snow cover, and solar altitude.

Snow cover caused the most significant diminution of radiation. A 3-cm wind-packed snow layer over 28 cm of clear ice reduced radiation transmittance from the clear to the snow-covered ice by up to 90 percent. During periods of snowmelt, radiation transmittance through snow-covered ice surfaces increased slightly. Moderate diurnal variations in radiation transmittance (about 5 percent) are attributed to solar altitude changes and associated changes in the direct-diffuse balance of solar radiation combined with the type of ice surface studied. Variations in radiation transmittance of nearly 20 percent over short periods of time are attributed to abrupt changes from a clear to a cloudy atmosphere. Areas disturbed by snowmobiles showed little difference in radiation transmittance from surrounding undisturbed areas.

Diffuse extinction coefficients varied from 0.006 for clear ice to 0.059 for a clear ice-refrozen slush ice combination. One higher diffuse extinction coefficient, 0.067, was noted at a surface disturbed by a snowmobile. Under-ice irradiance with depth was also measured on selected days.

A two-layer reflectance-transmittance model is used to illustrate the interaction of layers in an ice cover such as snow or frost overlying clear ice. Upper layers of high reflectance are shown to have considerable effect on the overall transmittance and reflectance of an ice cover. The model illustrates the wide range of effects of natural ice layering on overall transmittance and reflectance values.

The information on radiation transmittance from this study should prove useful to both groundbased and remote sensing investigations that seek to assess the status of winter biological activity, such as current or predicted winterkill, on lakes.

## 1. INTRODUCTION

The amount of radiation penetrating an ice or a combined ice and snow cover is often critical to the survival of plants and animals in both large and small freshwater lakes. In spite of the importance of this problem, the nature and magnitude of radiation penetration through ice is only partially understood. Comprehensive understanding has been hampered by unrepresentative measurements due to instrumentation and measurement technique problems.

With increasingly sophisticated remote sensors it is possible, under certain conditions, to identify various ice and snow types from satellites or aircraft. If additional ground-based information were available on the amount of radiation contributing to photosynthesis that penetrates various ice types, assessing the well-being of aquatic life during winter through remote methods would become possible. Significant new information on radiation transmittance through ice in the photosynthetically active range (400-700 nm) has been collected and is reported in this study.

Transmittance is here defined as the ratio of transmitted to incident radiation. Hemispherical transmittance is reported unless otherwise noted. Some investigators have discussed transmittance in the "visual" range. A careful review of these studies shows that some of the measurements correspond to luminous transmittance or transmittance from sensors that approximate the response of the human eye, while other studies use instruments that cover the 400-700 nm spectral range but do not correspond to the human eye response. Results of the latter category of studies are termed visible wavelength transmittance. Reflectance is defined as the ratio of reflected to incident radiation, with hemispherical reflectance reported unless otherwise noted.

The extinction coefficient is here defined as a measure of the space rate of diminution of any transmitted electromagnetic radiation through a homogeneous medium and does not imply the response of the human eye in its reception of radiation. The term "luminous extinction coefficient" might properly be used to define calculations from sensors with such a response. The term attenuation coefficient is used by some for radiation diminution in the 400-700 nm range, but this practice is ignored here. The diffuse extinction coefficient is introduced later in this report. The use of the term extinction coefficient as opposed to the diffuse extinction coefficient in conjunction with snow and ice data was considered inappropriate since these substances are not normally homogeneous in a natural state and are not comparable to substances such as pure water.

A comprehensive review of the results of radiation transmittance studies is presented in Maguire (1975a) (Table 1). To emphasize the diversity of measurement systems and techniques, some of the studies listed in Table 1 are reviewed below. Croxton, Thurman, and Shiffer

(1937) discuss using a "light-meter" to determine the intensity of "illumination." No specific characteristics of the instruments are given and presumably the values in Table 1 are for luminous transmittance. Greenbank (1945) fabricated a system using selenium photocells with filters for the "green, red, and blue ranges." Exact response of the unit is unspecified. His measurements of snow, ice, and water "light transmission," which can be tentatively categorized as visible wavelength transmittance, are too extensive to be completely reproduced here and are probably not comparable to most other measurements discussed. Wright (1964) measured "light attenuation with a photometer set calibrated in visible langleys/min . . . against an Epply pyrheliometer" in the 380-720 nm spectral range. The results seem to correspond to visible wavelength transmittance. Snow, ice, and water transmittances were measured on 15 days over a 3-month period. Saijo and Sakamoto (1964) calculated luminous transmittance using a selenium photocell with a "neutral density filter." Under-ice biological activity is discussed in their report. Halsey (1968) used a GM Manufacturing Company "photometer." Measurements are in "lux" and the values in Table 1 are luminous transmittances.

Goldman, Mason, and Hobbie (1967) used a Whitney Instruments irradiance "photometer" with surface and under-ice units, each equipped with a "Weston Photronic photocell." Schott RG-1, VG-9, and BG-12 filters, for which the spectral transmittances are well known, were used, but the response characteristics of the photocells or the photocells with filters are not given. The quality control and techniques employed appear to be excellent, but comparability of the measurements is meaningless without additional data on instrument characteristics. It is unclear whether the transmittance in Table 1, for an unfiltered photocell, is luminous transmittance or visible wavelength transmittance. Given in the report are transmittances ranging from 16 to 19 percent through 308 to 346 cm of ice for the unfiltered photocell, in addition to transmittance values using the filters.

Anderson (1970) used two instruments of different manufacture to measure "incident light" (Sekonic photometer) and "light penetration into the water (modified underwater photometer)." The "photometer" consisted of a selenium photocell sensitive to radiation in the 350-700 nm range. Filters used were Schott BG-7 (300-600 nm), Chance Pilkington 0 Gr-1 (450-600 nm), and Schott RG-2 (590-835 nm). It is possible to determine the characteristics of the filters, but the spectral responses of the selenium photocells are not given. Photometric units are used to describe the data, and the values in Table 1 are presumed to approximate luminous transmittance. The use of dissimilar instruments above and below the ice casts doubt on the accuracy of the transmittance values.

Schindler and Nighswander (1970) used a Gemware "light-meter (barrier layer photocell)" to measure "submarine light" and a Belfort "pyrheliograph" to measure "incident solar radiation." If these descriptions are taken literally, the above-ice measurements correspond to the total solar

Table 1. Transmittance of Radiation Through Ice and Snow (After Maguire, 1975a)

Ice thickness (cm)	Quality	Snow thickness (cm)	Quality	Luminous or visible wave-length transmittance (%)	Reference
10.2				86	Croxton, Thurman, and Shiffer (1937)
15.2				66	Croxton, Thurman, and Shiffer (1937)
35.6				33	Croxton, Thurman, and Shiffer (1937)
40				58	Chandler (1942)
7 11.4	slush cover			65	Zinn and Ifft (1941)
19	clear			84	Greenbank (1945)
17.8	clear	2.5	dry, light	2.5	Greenbank (1945)
19	partly cloudy			22	Greenbank (1945)
24.1	milky			14.4	Greenbank (1945)
24.1	milky	2.5	dry, light	1.1	Greenbank (1945)
40.6	fairly clear	16.5	crusted	0.1	Greenbank (1945)
27.3	very cloudy			7.2	Greenbank (1945)
31				30	Wright (1964)

Table 1. (Continued)

40				42	Wright (1964)
40		10		4.8	Wright (1964)
41		29		0.2	Wright (1964)
25				37	Saijo and Sakamoto (1964)
45				40	Saijo and Sakamoto (1964)
37	half clear,	8		0.01	Halsey (1968)
	half cloudy				
40	half clear,	15		0.01	Halsey (1968)
	half cloudy				
42	36-m clear,	1		50	Halsey (1968)
	6-m cloudy				
400				21	Goldman, Mason, and Hobbie (1967)
100		15		16	Anderson (1970)
75		50		13	Anderson (1970)
100		50	wet	5	Schindler and Nighswander (1970)
220		10-15		1-2	Schindler et al. (1974)

spectrum and the under-ice measurements to the 400-700 nm range. The accuracy of such transmittance values is clearly questionable. In a later paper, Schindler et al. (1974) used both a Belfort "pyrheliometer" and a Yellow Springs "pyranometer" located 2 km from the lake to measure incident radiation. Fifty percent of the measured solar radiation was considered to fall in the "visible portion of the spectrum." "Subsurface irradiance" was measured with a GM "submarine photometer" and a Weston selenium photocell. Filters were used occasionally. The measurements are more extensive than indicated by Table 1, but the use of dissimilar above-and under-ice instrumentation casts doubt on the accuracy and comparability of the data set. It should be mentioned that the term pyranometer is currently used to identify an instrument that measures direct plus diffuse radiation over the entire solar spectrum. The term pyrheliometer is currently reserved for an instrument that measures only direct solar radiation over the entire solar spectrum, but it was used in the past as the term pyranometer is currently used. It is presumed that the Belfort "pyrheliometer" is merely a pyranometer of early manufacture.

The above discussion indicates the wide range of instrumentation employed by numerous investigators. The various systems, both individually fabricated and commercially available, have produced results that are not comparable. The instruments selected for this study are patterned after an instrument designed, improved, and extensively tested by the Scripps Institute of Oceanography. They are commercially available and in wide use, although because they were introduced only recently, many investigators have not yet published their results (personal communications). Comparisons between data acquired by other investigators and the data acquired here are confined to one known published study using the same instrumentation as used here (Maguire, 1975b). Maguire's results of radiation measurements through ice in the 400-700 nm range are presented as diffuse extinction coefficients (Table 2). Further discussion of these data is contained in the analysis portion of this report.

Table 2. Diffuse Extinction Coefficients for Ice and Snow in the 400-700 nm Range (After Maguire, 1975b)

Medium	$k(\text{cm}^{-1})$
Ottawa River water	0.015
Clear ice	$0.02 \pm 0.003$
Cloudy ice	$0.20 \pm 0.03$
Soft new snow	$0.10 \pm 0.02$
Hard powder snow	$0.50 \pm 0.05$

The purpose of this study was to compile information on 400-700 nm radiation transmittance through some ice types common to the Great Lakes region. Response characteristics of the instruments are given later in this report. In the interest of brevity, the visible wavelength transmittance values calculated from these sensors will be called transmittance. The majority of the tests were conducted at a small inland lake located near Ann Arbor, Michigan (42°18' N, 83°43' W). A limited number of readings were collected near Whitefish Point at the eastern end of Lake Superior (46°46' N, 84°57' W). Data were gathered on the variation of radiation transmittance due to different types and thicknesses of ice and snow, solar altitudes, cloud types, and cloud amounts. Both natural snow-free and snow-covered ice surfaces, as well as artificially cleared (of snow) ice surfaces, were examined. A snow-free surface was desirable since radiation transmittance characteristics through snow are relatively well known when compared with the information available on radiation transmittance through ice. It is felt that if radiation transmittance through ice is better understood, then in natural, combined ice-snow surfaces both snow-free ice and snow values can be artificially integrated to obtain a good approximation of the natural radiation transmittance of a large area by high speed methods such as remote sensing.

## 2. INSTRUMENTATION AND TEST PLAN

Quantum sensors, manufactured by the Lambda Instruments Corporation, were used to measure radiation in the 400-700 nm band. A model LI-190S sensor was used to measure incoming radiation and a model LI-192S mounted on a specially designed arm was used to measure under-ice radiation. Figure 1 shows the above-ice sensor equipped with a mounting and leveling fixture. Details of the underwater sensor are shown in Figure 2. Detectors for both sensors are silicon photodiodes with enhanced response in the visible spectrum. Interference filters combined with detector characteristics produce sharp cutoff at approximately 400 and 700 nm.

The relative spectral sensitivity of the two sensors was determined by the manufacturer using a monochromator with a 2.5-nm band width and a thermopile with uniform spectral response over the 400-700 nm range to monitor the irradiance of the monochromator. The relative spectral response for each of the sensors is shown in Figure 3. Peak absolute responsivity of the under-ice sensor is  $0.037 \mu\text{amp/Wm}^{-2}$  at 670 nm and  $0.058 \mu\text{amp/Wm}^{-2}$  at 630 nm for the above-ice sensor.

Calibration was accomplished using a light source calibrated against a National Bureau of Standards lamp. The photon flux density of the standardized quartz halogen lamp was known in terms of  $\mu\text{einstains m}^{-2} \text{s}^{-1}$  where one  $\mu\text{einstein}$  equals  $6.023 \times 10^{17}$  photons. Certificates of calibration supplied by the manufacturer indicate an output of  $6.13 \mu\text{amp}/1000 \mu\text{einstains m}^{-2} \text{s}^{-1}$  for the underwater sensor and  $9.60 \mu\text{amp}/1000 \mu\text{einstains m}^{-2} \text{s}^{-1}$  for the atmospheric sensor.

Figure 1. Incident radiation sensor equipped with leveling unit.

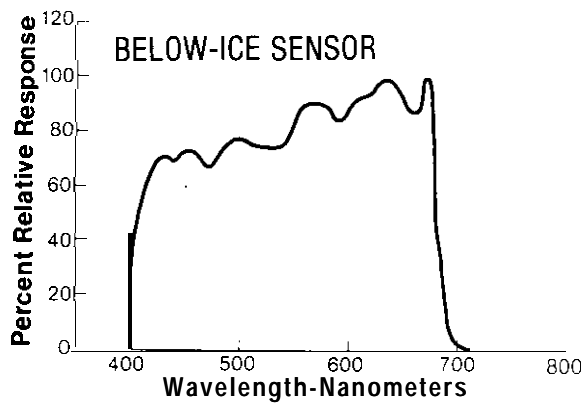
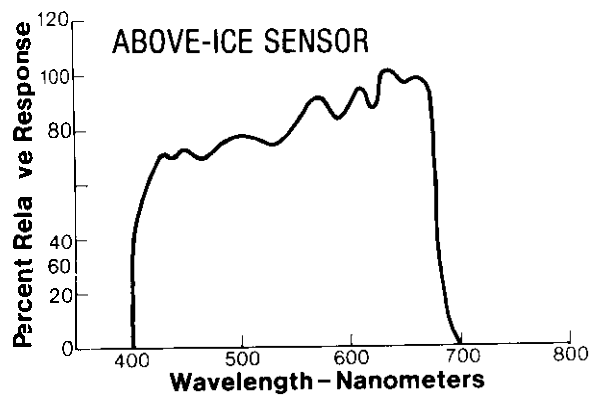
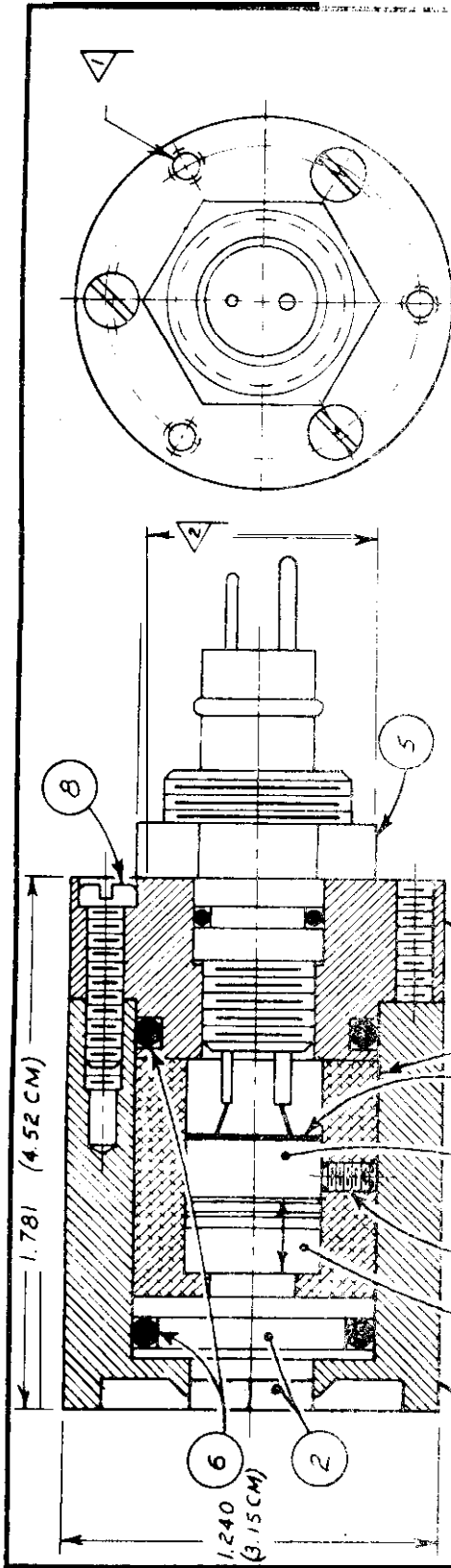


Figure 3. Relative spectral response of the two sensors used in this study.



NO.	DESCRIPTION	QTY	MATERIAL	FINISH	DRW. NO.
10	PHOTO-DIODE	1			
9	DIFFUSER	1			
8	RETAINING SCR.	3	MONEL	6-32UNC x .5	0907744
7	SET SCR.	1		4-40UNC x .12	0907743
6	O RING	2		NATIONAL NO. 622712	0907742
5	CONNECTOR	1		MARSH & MARINE NO. XSF-BCL	0907741
4	FILTER HOUSING	1	ALUMINIUM	.810 DIA x .804	
3	CAF	1	AMPCO 8	1.24 DIA x .609	
2	STE 7/DIFFUSER	1	MEMORAGG	.811 DIA. x .375	
1	HOUSING	1	AMPCO 8	1.24 DIA x 1.375	
NO.	NAME	QTY	MATL.	NOTES OR QFD	DRW. NO.

LAMBDA INSTRUMENT CORP. "LI-COR"  
 LINCOLN, NE USA

APPROVED BY: \_\_\_\_\_  
 DRAWN BY R.R.H.  
 REVISED \_\_\_\_\_

SCALE: 2" = 1"  
 DATE: 9-14-74

UNDER WATER SENSOR

DRAWING NUMBER  
 0918741

Figure 2. Underwater sensor assembly details (from Lambda Instruments Corporation, Instruction Manual for Li-Cor Quantum Sensors).

Cosine correction of the sensors is accomplished by means of a plexiglass diffuser (Fig. 2). Spectral shifts due to light entering the interference filter at oblique angles are eliminated by fitting the head with a collimating system. Cosine response as supplied by the **manufacturer** for an underwater sensor in both air and water is shown in Figure 4.

Smith (1969) has described the immersion effect on a diffusing material submerged in **water**. The response of wet and dry *collectors* of the same design differ, since a wet collector loses energy that in the dry collector is internally reflected back to the detector. The effect is caused by the change in the index of refraction at the boundary of the diffuser when it is immersed in water, causing a larger percentage of the incident flux to be backscattered into the water than into the air. Since all of the sensors are calibrated in air, a correction factor must be applied to all underwater readings. An immersion **correction** factor of 1.34, as recommended by the manufacturer, is applied to all data in this study.

The underwater sensor was mounted on an "L-shaped" arm of 1-1/4 inch white plastic pipe (Fig. 5) fabricated specifically for this study. The pipe was liberally perforated for ease in submerging the unit. The level of the sensor at the end of the arm was adjustable with respect to an above-ice spirit level. A platform to hold the "L" arm in a stable position was fabricated from clear plexiglass to minimize attenuation of incident light. For leveling, three large screws were positioned at each end of this triangular shaped platform.

Sensor output was measured by a Lambda Instruments Model LI-185 Quantum Radiometer-Photometer. The instrument features a solid state chopper stabilized amplifier providing a low impedance load to the sensors, resulting in *good* linearity. The unit was battery operated and completely portable (Fig. 6).

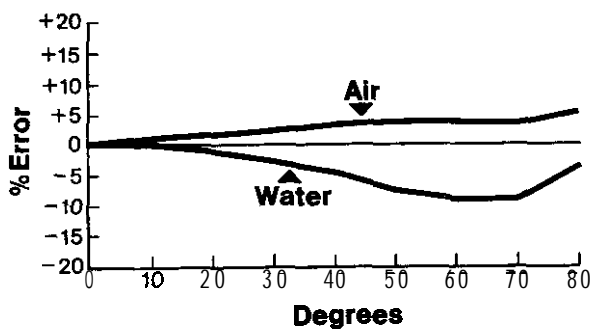


Figure 4. Cosine response of typical underwater sensor (from Roemer and Hoagland, 1977).

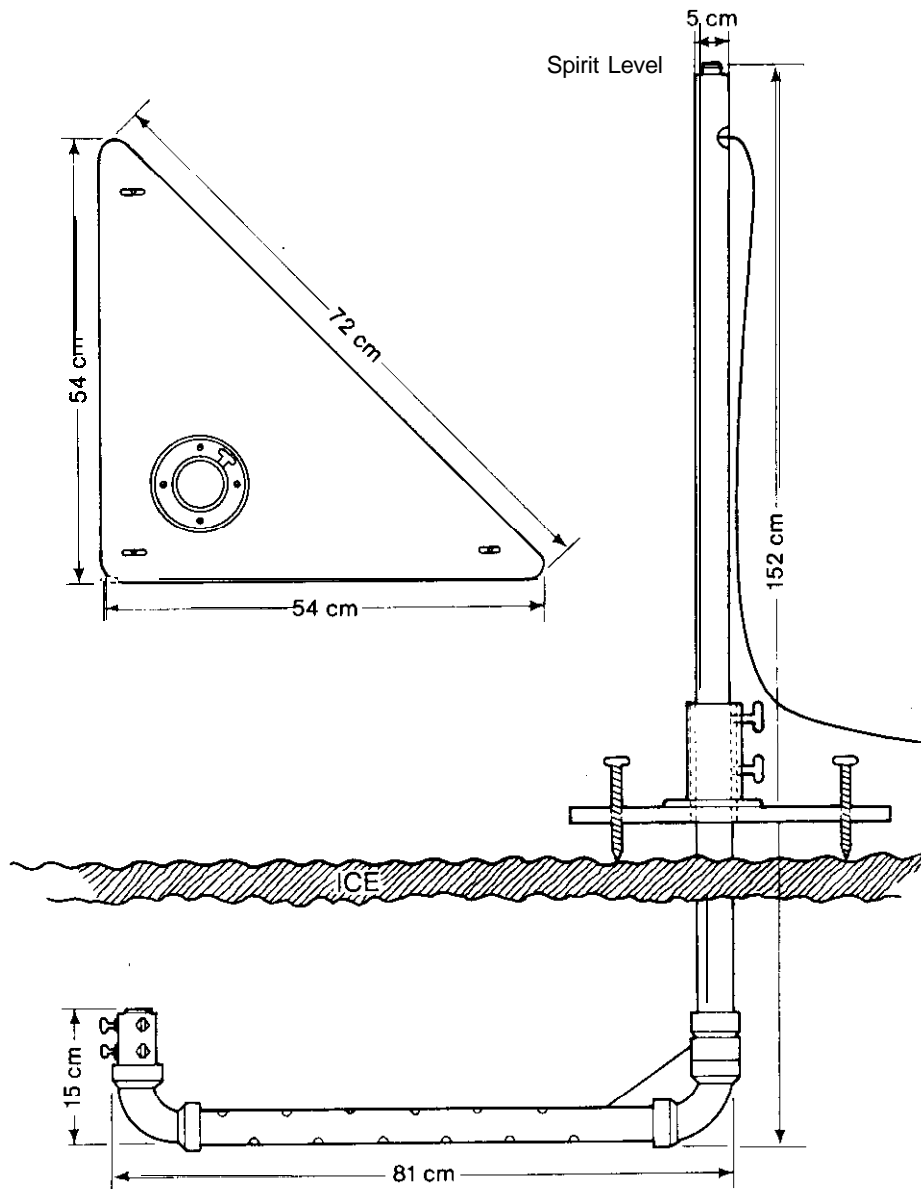
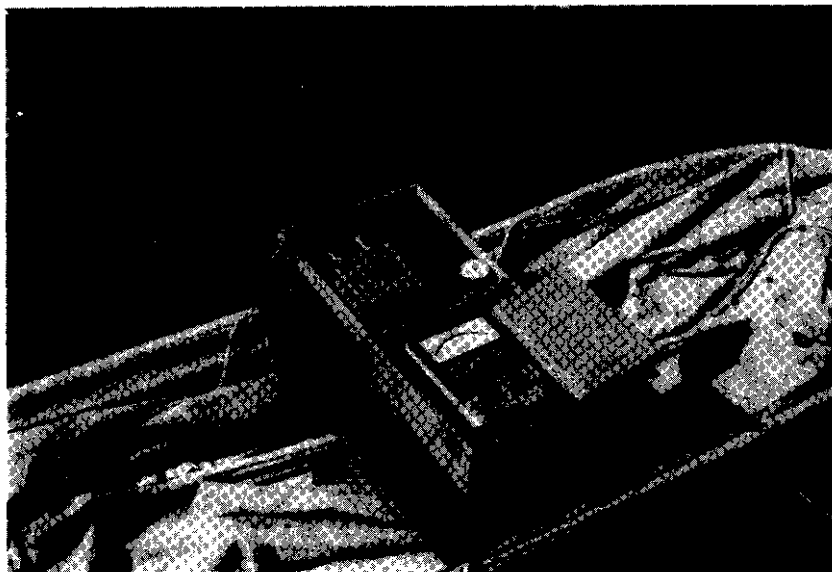


Figure 5. Design details of the support arm for the underwater sensor.



*Figure 6. Microammeter used for sensor readout and associated deck-to-sea switch.*

Although the sequence of events varied from one field trip to another, a "typical" series of steps can be described. When the weather forecast indicated favorable conditions the following day (no snowfall), all equipment was inspected and packed into a fiberglass sled to facilitate easy transport across the ice in a single trip. A vehicle of sufficient size, such as a General Motors Corporation Suburban, was used to transport the equipment to the lake. The loaded vehicle was left out-of-doors overnight, allowing the detectors and readout system to become adjusted to the ambient temperature, thus eliminating fogging of the optics and false readings of battery strength from the microammeter.

After a suitable site was selected, a 15-cm diameter hole was drilled with a power auger. A shield fabricated from a 50-gallon oil barrel, sawed in half, was used near the hole to reduce the possibility of scattering foreign ice chips over the area where the underwater portion of the "L" extension would be located (Fig. 7). After drilling, all equipment was moved a considerable distance away from the measurement site. The support arm was lowered into the hole and leveled, and some of the ice chips were pushed back into the hole where the support arm was located.

The topside sensor and mounting fixture were leveled on a small piece of plywood on the surface of the ice, about 5 m from any obstructions. Notations were made in a logbook on the type and thickness of ice, site conditions, prevailing atmospheric conditions, and the above-and under-

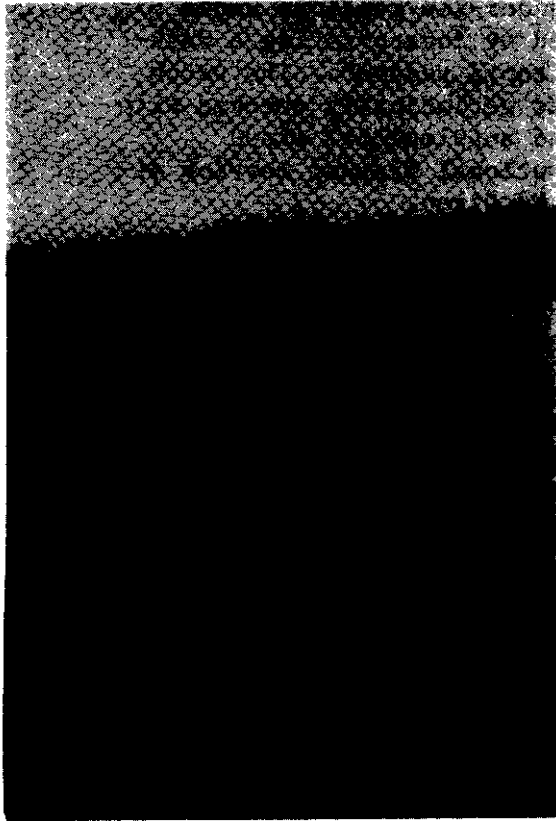


Figure 7. Overall and closeup views of drilling operations with barrel shield.

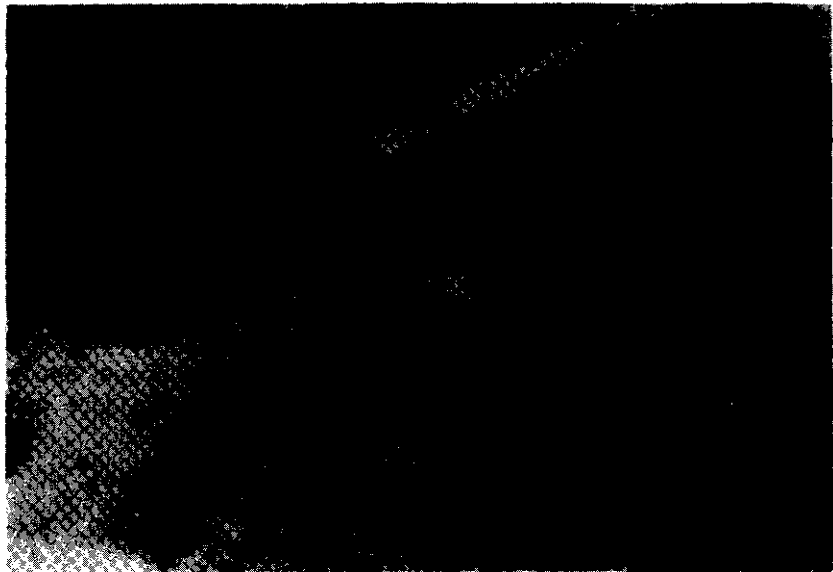


Figure 7. No. 2

ice readings. Completion of both above-and under-ice readings under similar atmospheric conditions was facilitated by incorporating a **deck-to-sea** switch into the electronics to insure rapid readout. The watch used to determine the time of each reading was periodically checked with a time-standard radio signal. Temperature and supplemental cloud observations are from hourly records of the National Weather Service at the Detroit Metropolitan Airport in Romulus, Michigan.

### 3. DATA REDUCTION

Above-and under-ice readings and pertinent field notes were transcribed on computer cards at the end of the field season. Subsequent processing included application of appropriate calibration factors and computation of ratios of under-ice to above-ice radiation. The local standard time (LST) of each observation was converted to true solar time (TST) as follows:

$$TST = LST + 4(\lambda - \lambda_s) + E, \quad (1)$$

where

$\lambda, \lambda_s$  = meridian of the observer and standard meridian, respectively,  
 $E$  = equation of time.

The solar altitude,  $\gamma$ , at the time of each observation was determined for the local latitude from

$$\sin \gamma = \sin \phi \sin \delta + \cos \phi \cos \delta \cos h, \quad (2)$$

where

$\phi$  = latitude,  
 $\delta$  = declination of sun,  
 $h$  = **hour angle** = (TST - 1200) • 15".

This was developed by using an electronic computer and methods described by Bolsenga (1968). A computer program was developed to produce graphics of transmittance against TST in addition to associated listings of transmittance ratios, ice composition, atmospheric conditions, **site** water depth, sensor depth, TST,  $\gamma$ , and zenith angle of the sun. A computer was also used to calculate the diffuse extinction coefficients and values for a two-layer model described in the analysis.

#### 4. ANALYSIS

##### 4.1 General

The ice surfaces observed in this study were classified as clear, refrozen slush, and brash ice. Clear ice and refrozen slush ice often occurred in combination. Refrozen slush ice is similar in appearance to snow ice, but the method of formation is different. Snow ice forms from snow loading an existing ice cover with upward water seepage through stress cracks in the old ice cover into the snow layer, which subsequently refreezes. Snow ice normally forms on small inland lakes such as Silver Lake. However, severe early season temperatures formed a thick layer of clear ice that did not fracture due to the snow load. Refrozen slush formed due to mild temperatures that reduced the snow cover on the lake to slush. Subsequent lower temperatures completely froze this slush into the snow ice-like substance called refrozen slush. Brash ice is an accumulation of loose fragments of ice randomly frozen together. Initially, thin ice forms in a sheltered bay or other quiet water area. On large lakes water movements break up, move, and compact this ice cover into brash unless extreme turbulence is encountered.

Ice types at each site are discussed in the following analysis. Brash ice was only encountered at Whitefish Point on Lake Superior. Dates and locations of the measurements are listed in Table 3.

*Table 3. Dates, Locations, and Surface Conditions of the Measurement Sites.*

Date	Location	Surface
12/22/76	Silver Lake	Natural
1/5/77	Silver Lake	Cleared
1/6/77	Silver Lake	Cleared
1/7/77	Silver Lake	Cleared
1/17/77	<b>Silver</b> Lake	Cleared
1/18/77	Silver Lake	Cleared
1/19/77	Silver Lake	Cleared
1/26/77	Silver Lake	Cleared & Natural
2/3/77	Whitefish Point	Natural
2/14/77	Silver Lake	Natural
2/16/77	Silver Lake	Natural
2/17/77	Silver Lake	Natural
2/22/77	Silver Lake	Natural
3/7/77	Silver Lake	Natural
3/8/77	Silver Lake	Natural
3/9/77	Silver Lake	Natural

It was necessary to clear snow from the ice on several occasions to obtain readings from the under-ice sensor and to acquire a certain number of snow-free readings as described earlier (Table 3). Cleared areas were roughly circular, 3 to 7 m<sup>2</sup> in area, and extended to the south of the borehole to minimize shadow effects on the underwater sensor. An ideal method to experimentally assess the effects on measurement accuracy of artificially clearing an area would be to progressively clear an extremely large area using both mechanized and manual equipment. The mechanical apparatus was not available, so the following more modest, but less conclusive, test was conducted.

Slightly over 1 cm of new snow covered a previously cleared area of nearly 37 cm of clear ice with about 2 cm of refrozen slush at the surface. After the first measurement of the day through undisturbed snow, the area was progressively cleared with a broom (Fig. 8). The effect on radiation transmittance is dramatically shown in Figure 9. The ratio of under-ice to above-ice radiation rose from 0.18, with undisturbed snow, to 0.66, with the area fully swept. Cloud conditions changed from 1/10 stratocumulus to 10/10 stratocumulus during site clearing. Solar altitudes ranged from 18 to 30° during the measurement period. The radiation transmittance values of the fully swept surface seem consistent with values for similar types and thicknesses of ice noted later. Most of the cleared areas were also larger than during this experiment. It is thus tentatively concluded that the artificially cleared areas provide radiation transmittance values that are representative except for possible shadowing effects of snow banks (discussed later). Additional experiments are necessary to verify this assumption. Measurements of natural (uncleared) ice surfaces are thus emphasized here.



*Figure 8. Progressive clearing of a measurement site to obtain the ratios shown in Figure 3.*

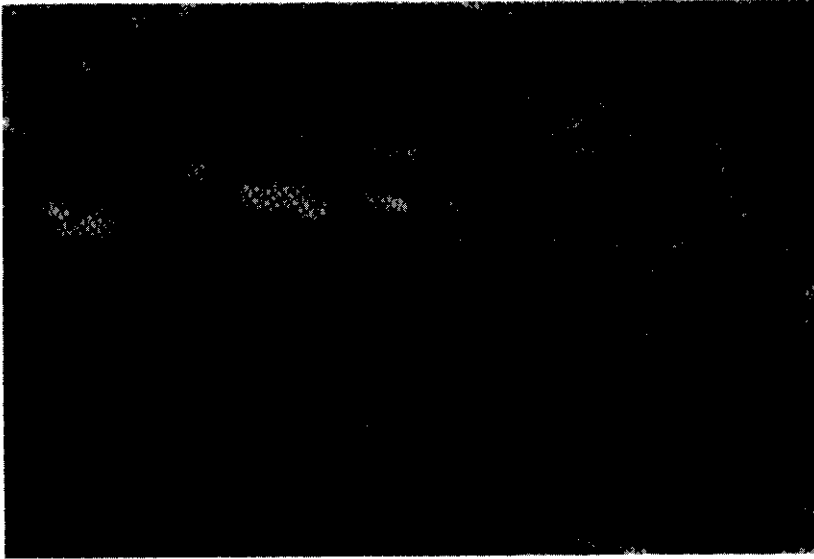


*Figure 8. No. 2*



*Figure 8. No. 3*



*Figure 8. No. 4*

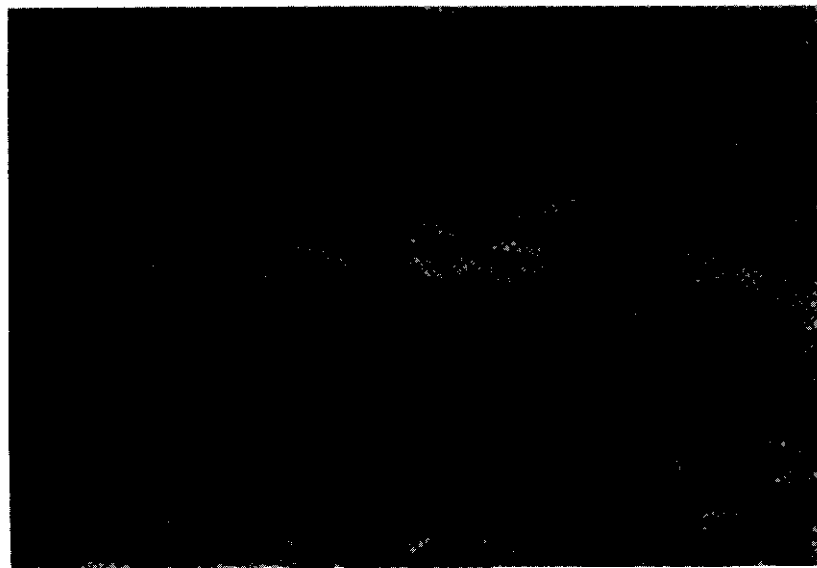


*Figure 8. No. 5*

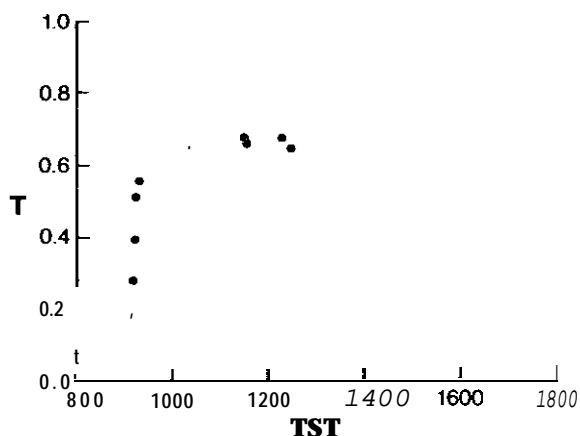


Figure 9. Ratio of under-ice to above-ice radiation ( $T$ ) versus true solar time ( $TST$ ) as the ice surface was progressively cleared of a thin snow layer, 26 January 1977.

#### 4.2 Daily Trends

A group of measurements were made from the same borehole by swinging the support arm at the ice-water interface from a clear ice area to a continuously snow-covered area. The ice thickness was 28 cm and the wind-packed snow was about 3-cm thick with an etched surface pattern. The sequence of measurements is shown in Figure 10. At 1038 TST a reading taken under the snow-free ice showed a ratio of transmitted to incident radiation of 0.80. At 1039 and 1040 TST the arm was moved to another area under the snow-free ice, yielding ratios of 0.77 and 0.82, respectively. The arm was next moved to the edge of the overlying snow surface where a ratio of 0.85 was obtained at 1041 TST. When the arm was moved completely under the snow, the ratios dropped to 0.08 and 0.10 at 1042 and 1043 TST. The same borehole was reoccupied at about 1200 TST. Ratios under the clear ice averaged 0.89 at one location and 0.83 at another. Under-snow ratios averaged 0.12. Sky conditions varied from 7/10 to 9/10 total sky cover with the *altocumulus* increasing towards the end of the period. Solar altitudes varied from 23 to 25". Figure 11 shows the sensor at the end of the support arm as photographed through the ice surface.

A series of measurements were taken on 3 consecutive days, during which 43 cm of ice (**combination** of refrozen slush and clear ice) deteriorated to 38 cm under mild weather conditions. On 7 March 1977, ratios of transmitted to incident radiation increased slowly from about 0.70 in the late forenoon to near 0.80 at about 1430 TST (Fig. 12). A small amount of snow was noted on the ice surface in the morning, but all snow had melted by 1400 TST, accounting for the increase in transmitted radiation. The readings continued to indicate ratios mostly under 0.80 on 8 March and 9 March 1977 (Figs. 13 and 14). Air temperatures during

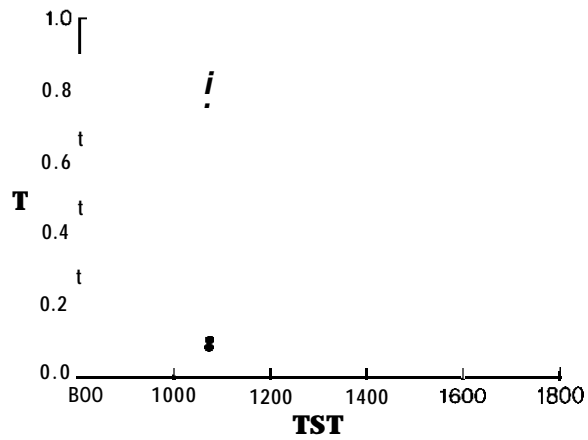


Figure 10. A series of measurements showing the contrast *between* radiation transmittance ( $T$ ) as a function of true solar time (TST) through ice *alone* and through the same ice cover with a snow layer, 22 December 1976.

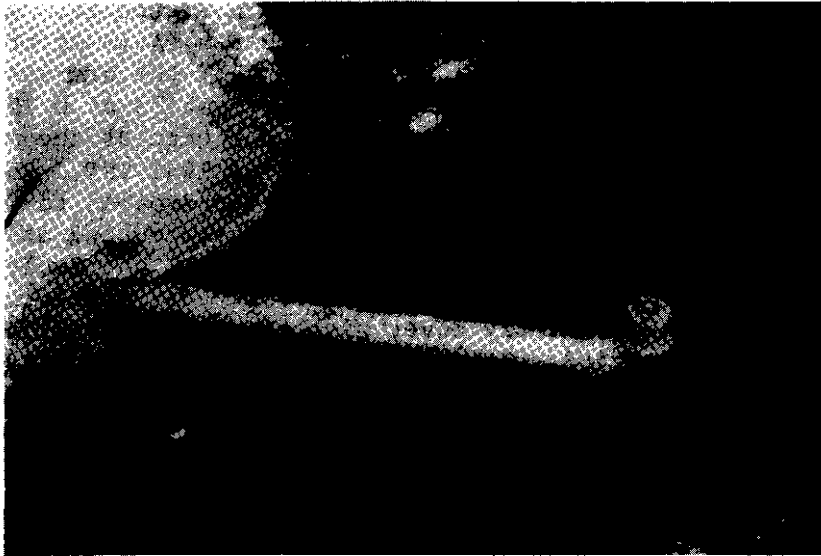


Figure 11. sensor and horizontal portion of boom as seen through the clear ice surface on 22 December 1976.

Figure 12. Ratio of below- to above-ice radiation ( $T$ ) as a function of true solar time ( $TST$ ) during a period of melting snow for 7 March 1977.

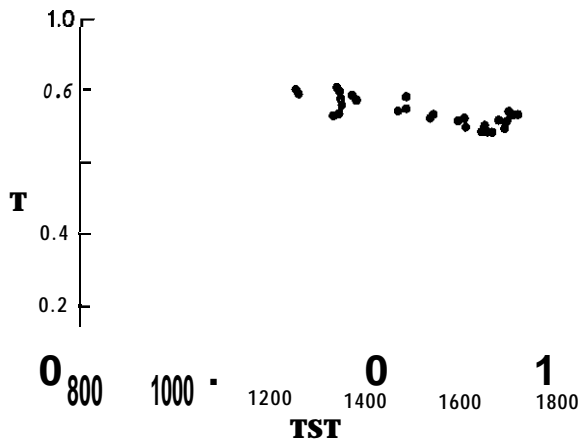
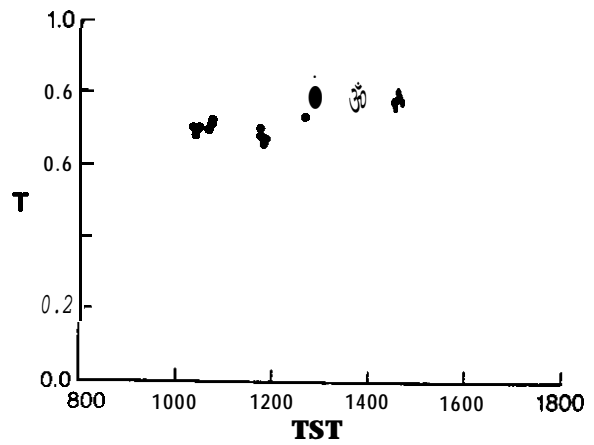
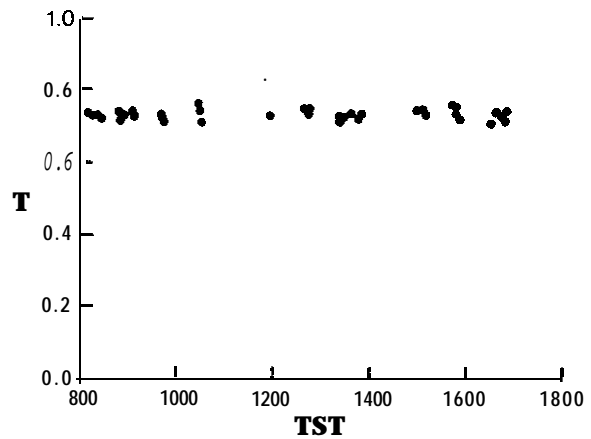


Figure 13. Radiation transmittance ( $T$ ) as a function of true solar time ( $TST$ ) during ice decay for 8 March 1977.

Figure 14. Radiation transmittance ( $T$ ) as a function of true solar time ( $TST$ ) during ice decay for 9 March 1977.



measurement periods at the Detroit Metropolitan Airport averaged 4.6" on 7 March 1977, 13.4°C on 8 March 1977, and 15.2°C on 9 March 1977. Cloud cover on 7 March 1977 remained at 6/10 stratocumulus throughout most of the day. On 8 March 1977, cloud cover remained at 3/10 cirrus throughout the day. On 9 March 1977, 3/10 cirrostratus in the morning increased to about 7/10 near the middle of the day. Near the end of the day, the cloud cover decreased to 3/10 altostratus. On 7 March 1977, solar altitudes during measurements varied from 31 to 43". Solar altitudes on 8 March 1977 varied from 8 to 42" and on 9 March 1977 from 11 to 45". Solar altitudes in this report were computed only during measurements. If measurements were not taken at 1200 TST, for example, maximum solar altitude for the day is not given. Therefore, maximum  $\gamma$  values on sequential days will not necessarily agree.

Other than the increase due to snowmelt on 7 March 1977, no other definite trend over the 2-day period is apparent even though temperatures remained high and caused a decrease in ice thickness. A diurnal trend indicated by the 9 March 1977 measurements is explained later. The dip and subsequent rise late in the day on 8 March 1977 might be owing to diurnal effects and instrument error due to low radiation levels, respectively. The lack of a smooth transition from low to high ratios on 7 March 1977 is due to raising and lowering of the under-ice sensor to obtain readings at various water depths. After each depth profile series, the arm could not be repositioned exactly and, since the ice surface and mostly likely the ice thickness were not entirely uniform, slightly different readings could be expected. The high readings on 7 March 1977 (0.82, 0.82, 0.85) at 1249, 1250, and 1255 TST, respectively, were taken immediately after profile measurements.

On 7 January 1977, measurements were taken from 1001 to 1549 TST at solar altitudes ranging from 7 to 26" (Fig. 15). Total sky cover varied from 0 to 2/10 cumulus during the period. The support arm was raised and lowered for depth profiles several times as follows:

- between the 1001 and 1006 TST readings,
- between the 1122 and 1128 TST readings,
- between the 1233 and 1245 TST readings,
- between the 1358 and 1442 TST readings, and
- between the 1527 and 1532 TST readings.

The ratios obtained for the period varied from 0.65 to 0.95, a 30 percent range in radiation transmittance. The significant difference can be attributed to movement of the arm to different locations under the ice cover, to differences in cloud cover, or to both effects combined. Such large variations were not noted on some other occasions when the support arm was raised and lowered, but possible larger differences in the thickness in addition to other characteristics of the ice at this site and cloud patterns might account for the wide variation. It is emphasized that the same borehole was used throughout the day.

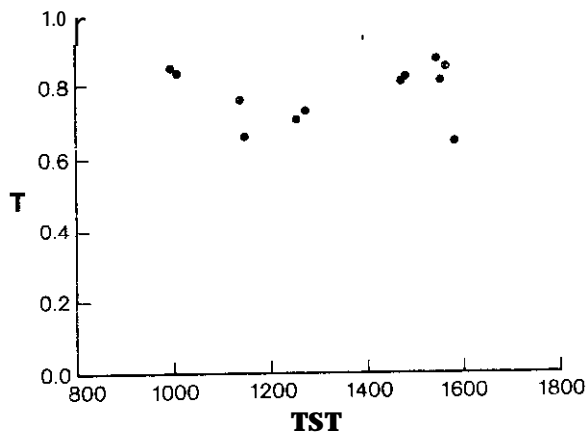
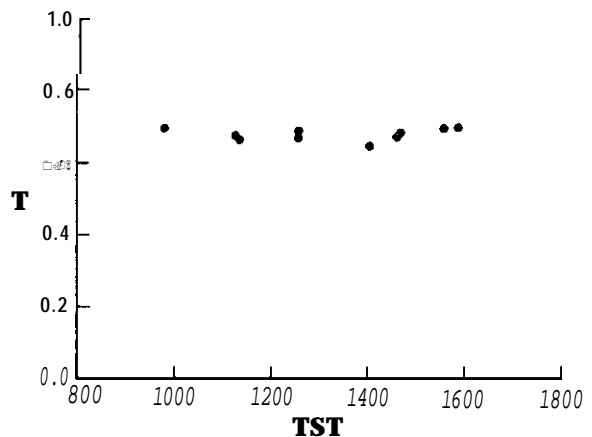


Figure 15. Radiation transmittance ( $T$ ) versus true solar time (TST) during a period of variable cumulus cloud coverage and during periods between depth profiles for 7 January 1977.

The readings on 9 March 1977 (Fig. 14) indicate that radiation transmittance might be affected by the solar altitude under certain conditions. In studies on reflectance over the entire solar spectrum of soils and crops, Idso and Reginato (1974), Idso et al. (1975), and Coulson and Reynolds (1971) found a significant rise in reflectance at low solar altitudes. The daily variation is most likely due to shadowing effects from a surface of complex nature, such as individual agglomerates of soil in a plowed field. A weak dependence of reflectance over the entire solar spectrum on solar altitude was found by Bolsenga (1977) and is attributed to the balance of diffuse vs. direct solar radiation and spectral reflectance characteristics of the particular ice cover. He speculates that slush ice and snow ice surfaces will exhibit higher reflectance at low solar altitude due to the increasing diffuse component of solar radiation early and late in the day combined with a high reflectance of slush and snow ice in the 400-700 nm range (Sauberer, 1938) and the fact that diffuse sky radiation is relatively rich in 400-700 nm range radiation. Observations on 9 March 1977, showing lower transmittance early and late in the day are consistent with these findings. Observations on 17 January 1977 (Fig. 16) show the opposite trend, with higher transmittance values early and late in the day. The apparent conflict can possibly be explained by the nature of the ice surfaces, which were clear ice on 17 January 1977 (36 cm) and refrozen slush on 9 March 1977.

Figure 16. Ratio of under-ice to incident radiation ( $T$ ) versus true solar time (TST) for a clear ice surface showing a marked difference between this diurnal pattern and the one observed for refrozen slush, 17 January 1977.



Another example of the influence of snow cover on radiation transmittance in the 400-700 nm spectral range is shown in Figure 17. A 5 to 8 cm thick snow layer covered 45 cm of ice composed of 4 cm of refrozen slush and 41 cm of clear ice. Temperatures during the measurement period at Detroit Metropolitan Airport were above freezing and varied from 6.1°C at about 1130 TST to 9.4°C at about 1645 TST. The snow was melting during this period. Cloud cover varied from 7/10 cirrus early in the measurements to 2/10-4/10 cirrus for most of the measurements to 6/10 cirrus at the end of the day. Radiation transmittance through the ice and snow layer increased at a steady rate from 0.06 at 1126 TST ( $\gamma = 38^\circ$ ) to 0.11 at 1640 TST ( $\gamma = 8^\circ$ ). The increase in transmittance is very likely due to snow melt. It should be noted that the change is opposite that attributed to solar altitude shown by the measurements on 9 March 1977 (Fig. 14), indicating that possible solar altitude influences are either completely masked by the effects of the snow melt, or that other factors such as shadowing or ice surface characteristics that might have been necessary for diurnal variation are lacking.

On 6 January 1977 (Fig. 18), measurements were taken through 29 cm of clear ice with a "pebbly" surface, artificially cleared of snow (shoveled and swept). Radiation transmittance averaged 0.83 during the period when solar altitudes during measurements ranged from 11 to 26°. Cloud cover was 6/10 stratocumulus and altostratus during most of the period. The transmittance values show a slight downward trend over the day, possibly due to shading effects of the cleared area. Measurements taken on the previous day, at the same site, at solar altitudes between 8 and 14° (1501 to 1543 TST), under clear skies, averaged 0.77. Measurements on 6 January 1977 at solar altitudes comparable to the previous day averaged 0.82. The difference could be due to changes in the ice surface, different atmospheric conditions, different shading effects, or to placement of the sensor at a different location under the ice. A minor amount of change in the surface on 6 January 1977 was noted in that the "pebbly" character disappeared by late in the day, but temperatures remained below freezing throughout the day. It should be noted that lower transmittance ratios associated with clear skies conflicts with the changes attributed to cloud cover below. Much additional work is needed on the effects of surface ice changes and atmospheric changes as related to radiation transmittance.

An ice cover 42 cm thick with 4 cm of refrozen slush overlying clear ice was examined on 14 February 1977. The refrozen slush was highly variable in surface characteristics and presented an opportunity to measure variations in radiation transmittance of the same ice cover at different positions in the same borehole (Fig. 19). The underwater sensor was located near the end of the meter stick shown in the photographs. The surface to the side of the support arm contained more snow lodged in a "pebbly" surface. The average of the ratios in the snow-free area was 0.58. The average of ratios in the partially snow-covered area only dropped to 0.53. Cloud cover during the period was fairly uniform at 9/10 stratocumulus. Solar altitudes varied from 29 to 35°. The measurements emphasize that the visual appearance of seemingly large surface differences in an ice cover does not always relate to large differences in radiation transmittance.

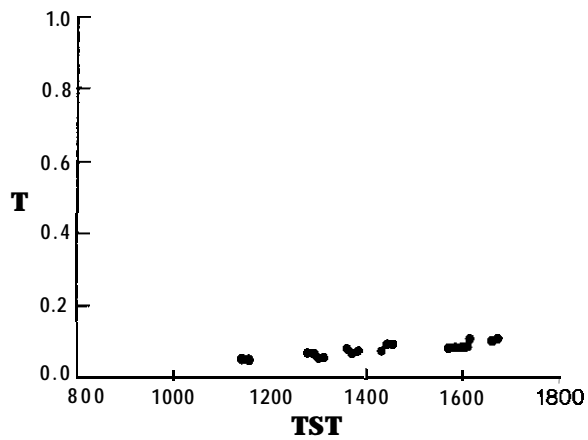


Figure 17. Increase in radiation transmittance due to snowmelt as indicated by the rise in transmittance ratio ( $T$ ) with true solar time ( $TST$ ), 22 February 1977.

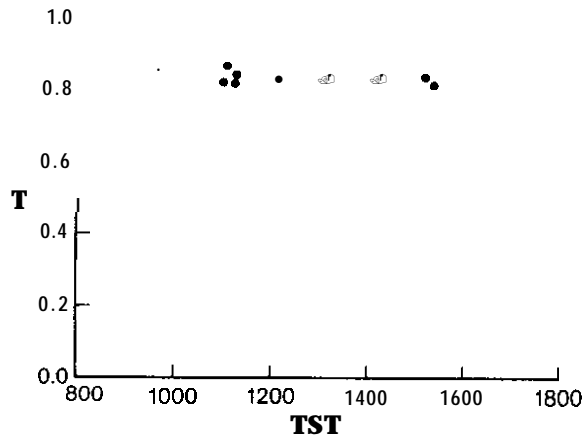
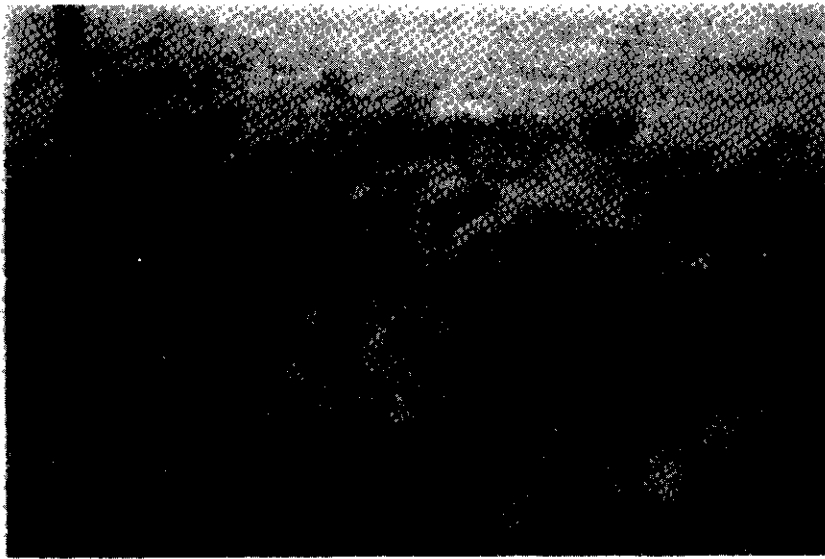


Figure 18. Ratio of under-ice to incident radiation ( $T$ ) versus true solar time ( $TST$ ) on a partly cloudy day with a changing ice surface, 6 January 1977.



*Figure 19. Highly variable surface characteristics of refrozen slush. The two surfaces are at different locations from the same borehole.*



The 18 January 1977 and 19 January 1977 site was also occupied on 17 January 1977. Solar altitude range was from 8 to 28". Thin high clouds, stratocumulus most of the day changing to cirrostratus late in the day, were noted. Total sky cover was 10/10 at the site. Light snow and blowing snow due to gusty winds occurred throughout the day. The variable, thin, high clouds caused large fluctuations in the microammeter needle during readings. It was felt in the field that readings could not be taken with enough speed to produce reliable ratios. However, Figure 16 indicates fairly steady ratios over the day. The ice was 36 cm thick and clear.

It is emphasized that on all 3 days (17 January 1977 through 19 January 1977) the same borehole was reoccupied and the support arm remained in the same position throughout the day, except for occasional leveling. Placement of the support arm at exactly the same spot was, of course, not possible on a day-to-day basis. The observations on these days show, on a preliminary basis, that radiation transmittance through clear ice is greatly affected by cloud patterns, which vary from clear to mostly cloudy (such as intermittent cumulus clouds). The previously discussed large variations in the ratios on 7 January 1977 might be due partially to the effect of cloud cover variations from 0 to 2/10 cumulus. On the other hand, totally overcast days showing some variability in the overall cloud pattern have little effect on radiation transmittance in this spectral range. Shading effects were observed in some of the observations, but it is believed that these effects are systematic and do not effect the changes reported as related to cloud cover.

A limited number of measurements were made on some relatively thick ice (56-64 cm) at Whitefish Point in Lake Superior (46°46'N, 84°57'W). A significant amount of blowing and falling snow prevailed during the Z-hour measurement period and could have adversely affected the above-ice readings for all data sets at this location. An average of five measurements taken near 1200 TST ( $\gamma = 28^\circ$ ) showed the ratio of under-ice to incident radiation through 64 cm of clear ice topped with a thin layer of frozen slush to be only 0.06. Two brash ice areas, both 56 cm thick, were measured with the overlying snow surface undisturbed and again after the surface was swept with a broom. At the first site, the ratio for the natural ice and snow surface averaged 0.07 and the swept surface averaged 0.15. At the second site, the unswept surface averaged 0.06 and the swept surface 0.08. The lack of significant increase in radiation transmittance at the second brash ice site can be explained by the extreme irregularity of the surface, which caused snow to remain in place between the brash ice blocks even after sweeping (Fig. 22). Solar altitude was about 27" at the first and 17" at the second brash ice site.

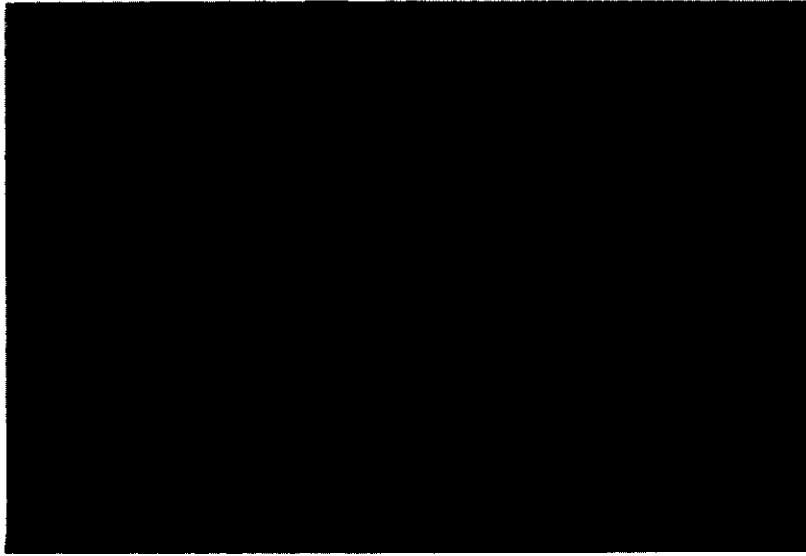


Figure 22. *Ice conditions at the second brash ice site showing snow trapped between the individual blocks of ice.*

#### 4.3 Snowmobile Disturbances

Measurements were also taken on surfaces disturbed by snowmobiles. On 16 February 1977, in an area of 46 cm of total ice with 3 cm of refrozen slush and 1 cm of granular metamorphosed snow undisturbed by snowmobiles, four transmittance measurements averaged 0.17. In an adjacent area, using the same borehole, measurements under a surface modified by a snowmobile track averaged 0.15. The ridge caused by the snowmobile consisted of about 3 cm of additional combined granular metamorphosed and normal snow (Fig. 23). Skies were clear and solar altitude varied from 29 to 30" during the period. To assess the effects of the possible flooding of such a surface due to either rain or conditions that might form snow ice (i.e., snow loading an existing ice cover, cracking, flooding, and refreezing) the surface was artificially irrigated. Radiation transmittance at the site not modified by the snowmobile rose from 0.17 to 0.44 and at the modified site from 0.15 to 0.49 (Fig. 24).

Additional measurements were made on 17 February 1977. At the first site the ice was 29 cm thick, including 3 cm of refrozen slush. About 2 cm of crusted, rippled snow overlaid the undisturbed area. Measurements in the undisturbed area showed an average transmittance ratio of 0.15. In the area modified by the snowmobile, the ratio was 0.14 (Fig. 25). Solar altitudes varied from 33 to 36" during the period. At a second site, with 52 cm of total ice, including 4 cm of refrozen slush, a snowmobile had operated in a slushy surface at the top of the ice, creating a "pebbly" ice and snow surface. Radiation transmittance



Figure 23. *Surface conditions at site used to measure radiation transmittance through a natural ice and snow surface and the same surface disturbed by a snowmobile.*

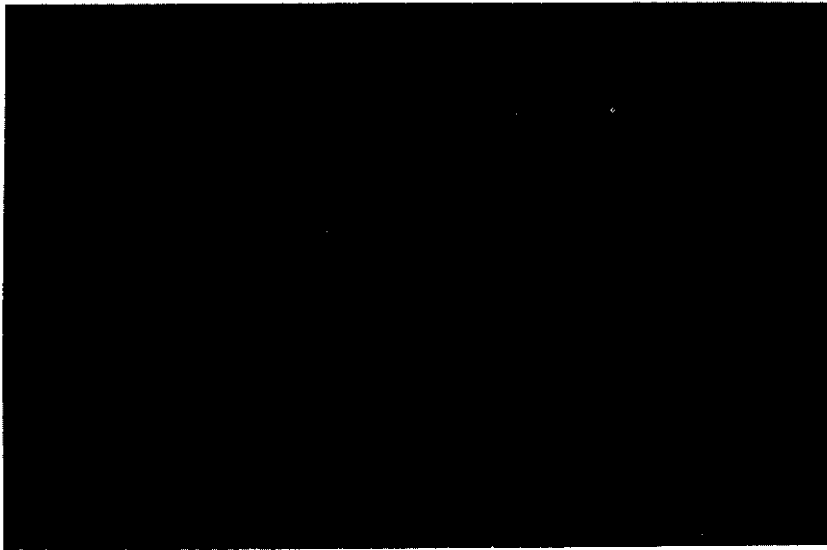


Figure 24. *Conditions at the site shown in Figure 23 after irrigation.*

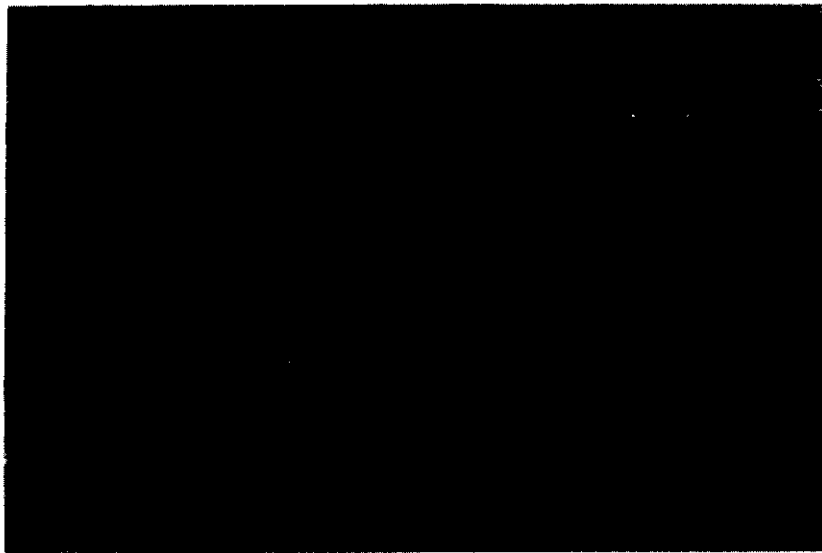


Figure 25. *Surface conditions at snowmobile track measurement site showing the undisturbed and disturbed areas and a closeup of the track imprint.*

averaged 0.23 at solar altitudes varying from 28 to 32". The general site area and a detailed view of the snowmobile track are shown in Figure 26. No measurements of the adjacent undisturbed area were taken for this case. Only light (0-2/10) altocumulus clouds were present during these measurements on 17 February 1977.



*Figure 26. overall and detailed views of snowmobile track measurement site.*

#### 4.4 Diffuse Extinction Coefficients

Diffuse extinction coefficients obtained from these data by

$$k = \frac{\ln E_0 - \ln E}{z} \quad (3)$$

where

$E_0$  = irradiance at surface,

$E$  = irradiance at depth,

$z$  = depth (cm),

and those obtained by Maguire (1957b) are combined in Table 4. In most cases, when a series of measurements on a given day was interrupted by any movement of the support arm, except for **releveling**, diffuse extinction coefficients were computed only from measurements before the movement. All diffuse extinction coefficients are the average of several individual measurements. If sufficient measurements under appropriate conditions were not available, a diffuse extinction coefficient was not computed.

Table 4. Diffuse Extinction Coefficients [ $k(\text{cm}^{-1})$ ] Obtained for Selected Situations in this Study and Coefficients Obtained by Maguire (1975b) for the Same Spectral Range.

##### a. CLEAR ICE

Date	$k(\text{cm}^{-1})$	Comments	Reference
1/6/77	0.006		This work
1/17/77	0.011	Blowing snow	This work
1/18/77	0.006		This work
1/19/77	0.008	Light snow	This work
	$0.02 \pm 0.003$		Maguire

##### Table 4b. BRASH ICE

Date	$k(\text{cm}^{-1})$	Comments	Reference
2/3/77	0.048	Snow between blocks	This work
2/3/77	0.052	Snow between blocks	This work

Table 4c. COMBINATION--REFROZEN SLUSH + CLEAR

Date	Site	k(cm <sup>-1</sup> )	Thickness-(m)			Reference
			TOT	SI*	Snow	
2/16/77	1	0.027	43	4	1	This work
2/17/77	2	0.027	41	2	T**	This work
2/16/77	3	0.037	39	4	o-2	This work
2/16/77	2	0.039	43	3	2	This work
2/17/77	1	0.054	45	3	3	This work
2/22/77	1	0.059	45	4	5-8	This work

\*SI = slush ice.

\*\*T = trace.

Table 4d. COMBINATION--REFROZEN SLUSH + CLEAR DURING DECAY

Date	k(cm <sup>-1</sup> )	Reference
3/7/ through 3/9/77	0.006 to 0.008	This work

Table 4e. SNOWMOBILE TRACKS

Date	Site	k(cm <sup>-1</sup> )	Thickness (cm)			Reference
			TOT	SI*	Snow	
2/16/77	2	0.041	46	3	4	This work
2/17/77	4	0.051	52	4	T**	This work
2/17/77	3	0.067	29	3	T**	This work

\*SI = slush ice.

\*\*T = trace.

Table 4f. SNOW

k(cm-1)	comments	Reference
0.10 ± 0.02	Soft new	Maguire
0.500 ± 0.05	Hard powder	Maguire

Diffuse extinction coefficients obtained here for clear ice ranged from 0.006 to 0.011. The values are lower than those obtained by Maguire. In addition, the highest values obtained here were during periods of light and blowing snow. Crack patterns and surface variations could possibly account for the differences. The two brash ice surfaces yielded about the same diffuse extinction coefficients. Considerable snow between the individual blocks was noted.

The combinations of refrozen slush and clear ice present the most complex diffuse extinction coefficient pattern noted. It is fairly obvious that the amount and condition of snow on the ice surface have a profound effect on the diffuse extinction coefficient magnitude. On 16 February 1977, conditions of the surface at site 1 were crusted granular snow with chips from the ice auger inadvertently sprayed **over** the surface. It is also possible that **some** of these chips were wet, but this was not noted in the logbook. On 17 February 1977, at site 2 the same diffuse extinction coefficient was obtained with less slush ice (0.027), but the ice surface was bumpy with depressions partially filled with granular snow. The surface was composed of 60 percent thin snow and 40 percent exposed ice.

The surface on 16 February 1977, at site 3 showed an irregular pattern of crusted snow and exposed ice with the snow varying from 0 to 2 cm. The diffuse extinction coefficient on 16 February 1977, at site 2 (0.039) was nearly the same as that computed for site 3 (0.037), but with the slush ice amount less and snow amount more than at site 3.

On 17 February 1977, at site 1 the diffuse extinction coefficient rose significantly **over** all previous values. The snow was crusted, granular, and uniform **over** the area. On 22 February 1977, the diffuse extinction coefficient remained nearly the same as that obtained on 17 February 1977, with significantly increased snow **cover**. However, field notes indicate that the thick snow cover on 22 February 1977 was irregular, causing higher radiation transmittance than with a uniformly thick layer.

During ice decay, diffuse extinction coefficients of combined refrozen slush and clear ice remained in a remarkably small range (0.006 to 0.008). Water was observed on the surface and percolating through the ice during portions of the period.

An apparent severe effect of snowmobiles operating on the ice and snow surfaces is shown by the high diffuse extinction coefficient values in Table 4. However, the previous section in this report and other values in Table 4 for the same date emphasize that differences between radiation transmittance at the disturbed and undisturbed sites were small. The range in the diffuse extinction coefficients is also small, but that lack of wide variation is most likely due more to site selection and limited data base than to actual conditions that could occur.

#### 4.5 Reflectance-Transmittance Model

It is important to note that the lack of homogeneity of most natural ice areas or combinations of ice and snow can produce diffuse extinction coefficients and transmittance values more representative of certain upper layers of an ice cover rather than the bulk of the ice cover. Situations occur where natural ice surface phenomena, such as surface etching due to windblown snow, frost accumulation or melting, microrelief due to melting, and fractures or internal bubble structure, are the rule rather than the exception. Transmittance values and diffuse extinction coefficients given here are usually the result of a combination of these factors and may be site specific.

The effect of layering on the overall transmittance and reflectance values of an ice cover can be estimated from a simple model. The reflectance and transmittance of each individual layer are used to obtain combined reflectance and transmittance values for the ice cover.

The combination reflectance,  $\rho(C)$ , of a two-layered system is

$$\rho(C) = \rho(A) + \frac{\tau^2(A)\rho(B)}{1 - \rho(A)\rho(B)}, \quad (4)$$

where

- $\rho$  = reflectance,
- $\tau$  = transmittance,
- A = upper layer,
- B = lower layer.

The combination transmittance,  $\tau(C)$ , of a two-layered system is

$$\tau(C) = \frac{\tau(A)\tau(B)}{1 - \rho(A)\rho(B)}. \quad (5)$$

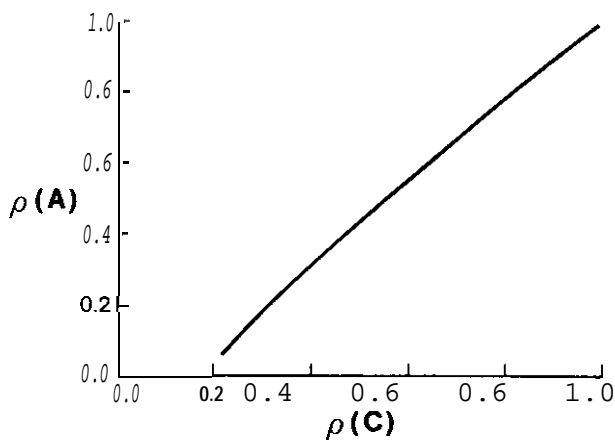
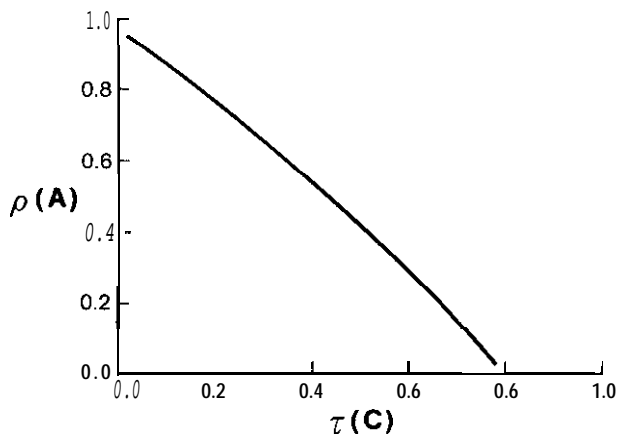
Details of the derivation of equations (4) and (5) and a sketch of the two-layer model are given in the Appendix.

To illustrate the effectiveness of the model, equations (4) and (5) were programmed to run on an electronic computer. Hypothetical ice-cover transmittance, reflectance, and absorptance values (layer B) were stipulated and held constant for each computer run, during which varying values were substituted for  $\rho$  and  $\tau$  in layer A (representing snow, frost, bubble layers, etc.). Layer A transmittance and reflectance values were incremented at 1-percent intervals.

In the first computer run, clear ice was simulated for the B layer using  $p(B) = 0.19$ ;  $\tau(B) = 0.80$ ; and  $a(B)$ , the absorptance, = 0.01. The reflectance and transmittance of the A layer were varied, with  $a(A)$  held constant at 0.01. Graphic displays of  $\rho(A)$  versus  $\tau(C)$  and  $p(A)$  versus  $p(C)$  are shown in Figure 27. The effects of a highly reflective upper (A) layer on such an ice cover are immediately apparent. A snow layer with a reflectance of 0.80 would yield  $\rho(C)$  of 0.81 and  $\tau(C)$  of 0.18. An upper layer of considerably less reflectance,  $\rho(A) = 0.20$  for example, would yield  $p(C) = 0.32$  and  $\tau(C) = 0.66$ . The highly reflective snow is obviously the dominant factor in the combination and the reflectance-transmittance values of the ice layer have little influence on the combination when snow is present. The example used here for a highly reflective snow cover overlying clear ice is similar to the experimental situation encountered on 22 December 1976 (Fig. 10), where  $\tau(B) \approx 0.80$ , in an ice-free area and  $\tau(C) \approx 0.10$  in an adjacent area covered by 3 cm of snow. Other field data, such as those shown in Table 4 and also discussed in the Analysis Section, verify the effects of snow cover on ice transmittance.

Figure 27. Upper layer reflectance,  $\rho(A)$ , versus combined transmittance,  $\tau(C)$ , and upper layer reflectance,  $\rho(A)$ , versus combined reflectance,  $p(C)$ , from operation **of** the two-layer model for a situation where the underlying layer simulates clear

ice.



In the second computer run, snow ice was simulated for the B layer with  $p(B) = 0.44$ ,  $\tau(B) = 0.45$ , and  $a(B) = 0.01$ . The reflectance and transmittance of the A layer were again varied with  $a(A)$  held constant at 0.01. The graphic displays are shown in Figure 28. A snow layer with a reflectance of 0.80 would yield  $\rho(C) = 0.83$ , nearly the same as for the clear ice case, and  $\tau(C) = 0.13$ . An upper layer of lower reflectance,  $\rho(A) = 0.20$ , would yield  $\rho(C) = 0.50$  and  $\tau(C) = 0.39$ . The high reflectance of the underlying snow ice produces a higher  $\rho(C)$  than for clear ice in a situation where  $\tau(A)$  is high. Field data corresponding to the snow ice model were not collected.

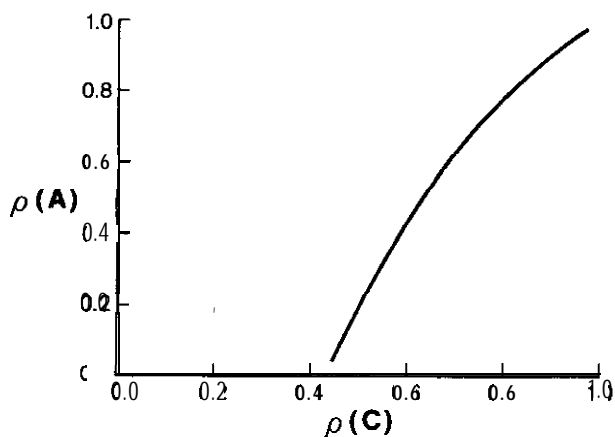
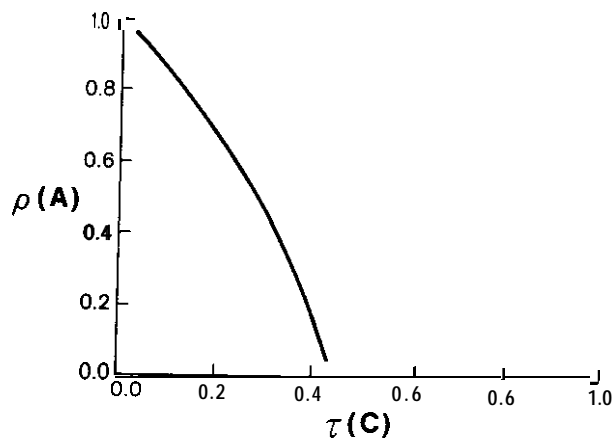


Figure 28. Upper layer reflectance,  $\rho(A)$ , versus combined transmittance,  $\tau(C)$ , and upper layer reflectance,  $\rho(A)$ , versus combined reflectance,  $\rho(C)$ , from operation of the two-layer model for a situation where the underlying layer simulates snow ice.

The above two examples should be sufficient to illustrate the coupling effect operating on a layered ice system. Reflected radiation in the 400-700 nm range was not measured in this study, so it is not known whether the  $p(A)$  or  $\tau(A)$  values in the above discussion are representative. The  $p(A)$  values are from known values of ice reflectance over the entire solar spectrum. The reflectance of clear ice in the 400-700 nm range can be inferred from several of the transmittance measurements given here, including those shown in Figure 10. No transmittance measurements were taken through snow ice, but  $p(A)$  values for snow ice in the 400-700 nm range can be roughly approximated from transmittance values of about 0.55 taken on 14 February 1977 through 4 cm of refrozen slush overlying 38 cm of clear ice.

Additional verification of the model would be possible if detailed stratigraphy of the ice were available. Unfortunately, a coring auger acquired for that purpose proved defective on the first day of measurements. Future field data collection will include such information.

Notwithstanding the above assumptions, the magnitude of the coupling in a layered system is apparent from the computations. It should also be stressed that the ice covers studied here and in all other studies of natural ice represent layered systems to a greater or **lesser** degree.

#### 4.6 Depth Profiles

The primary purpose of this study was to measure radiation transmittance from the ice surface to the ice-water interface. Limited measurements of underwater radiation at various depths below the ice were also taken on selected measurement days. Underwater irradiance characteristics at various water depths are complex even without an ice cover and deserve detailed attention as described by Tyler and Smith (1970). The measurements given here of radiation under the ice at various depths are not designed to duplicate or enhance a study such as Tyler and Smith's. They are nevertheless presented because no measurements of this type are known to exist.

The design of the support arm permitted lowering the vertical pipe section through a sleeve in the leveling platform to any depth limited by the length of the vertical pipe. At the desired depth, thumbscrews were tightened and a reading taken with the **microammeter**. Measurement of sensor depth below the water-ice interface was by determining the length of travel of the vertical portion of the support with a meter stick. The method was crude and subject to inaccuracies. The **observations** are shown in chronological order in Figures 29 and 30. **Only** profiles under natural snow and ice surfaces are included.

Ice, atmospheric conditions, and solar altitudes during the profiles are given in Table 5. Most of the profiles show relatively smooth transitions from high ratios of underwater to above-ice radiation near the water surface to lower ratios at depth. The measurements on 22 February 1977 present an exception to this trend. Possibly the underwater

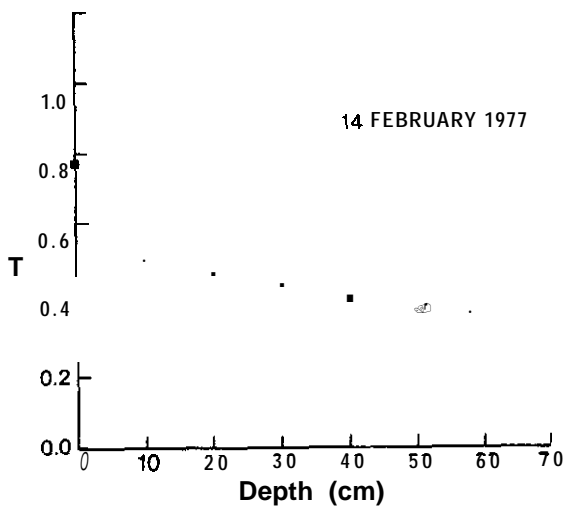
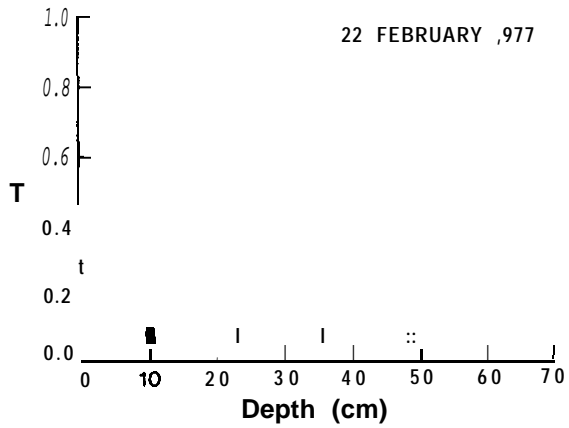
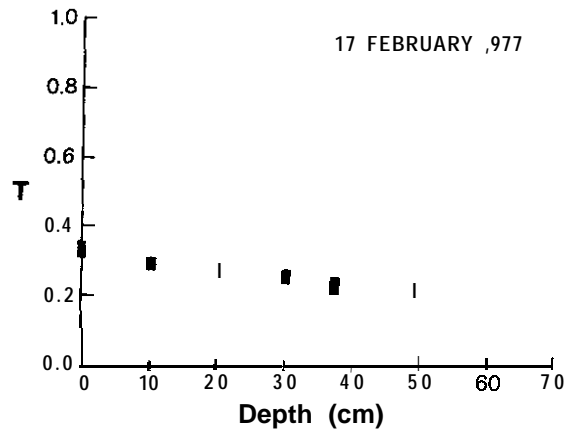


Figure 29. Radiation transmittance as related to depth for 14, 17, and 22 February 1977.



as related to depth for 7, 8, and 3 March 1977.  
 Figure 30. Radiation transmittance

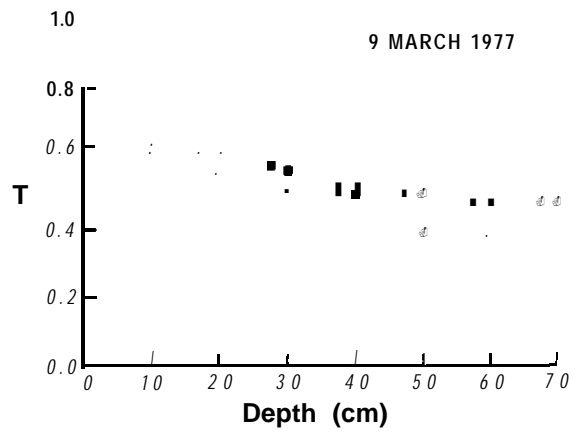
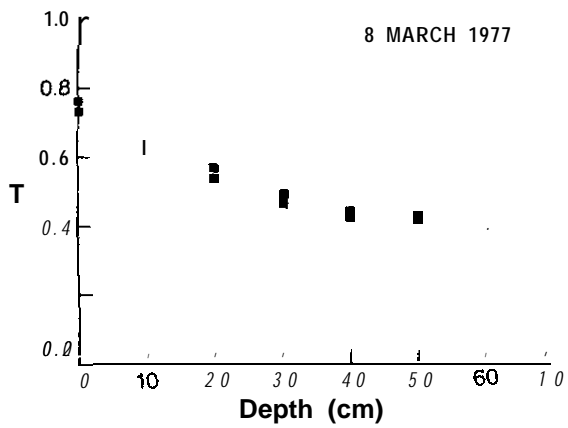
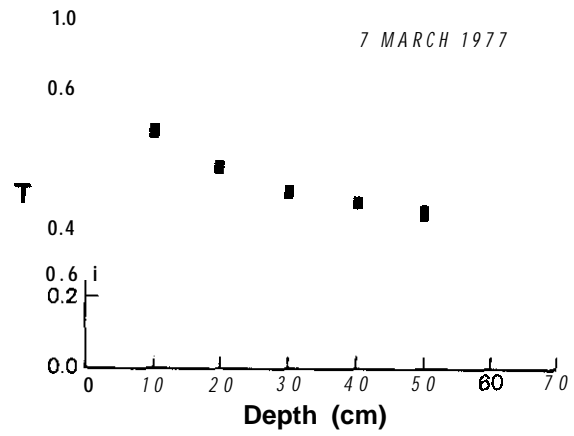


Table 5. Atmospheric Conditions, Solar  
Altitudes ( $\gamma$ ), and Ice Types During  
Depth Profiles

---



---

2/14/77	9/10 stratocumulus $\gamma = 32-33^\circ$ 38 cm clear ice 4 cm slush ice
2/17/77	0/10 clear $\gamma = 11-17^\circ$ 41 cm clear ice 1 cm slush ice 2 cm new plus granular snow
2/22/77	2-4/10 cirrus $\gamma = 28-36^\circ$ 41 cm clear ice 4 cm slush ice 5-8 cm snow
3/7/77	6/10 stratocumulus $\gamma = 39-41^\circ$ 43 cm combination clear and refrozen slush
3/8/77	3/10 cirrus $\gamma = 11-31^\circ$ Less than 43 cm - ice melting, some water on surface
3/9/77	3/10 cirrostratus - morning, 7/10 cirrostratus - midday, 3/10 altostratus - late afternoon $\gamma = 12-38^\circ$ 38 cm combination clear and refrozen slush

---

radiation levels were too low to permit meaningful profile measurements on that day. Figure 17 shows the low ratios obtained at the ice-water interface. On 9 March 1977, profile measurements at different times produced significantly different curves. Such behavior can be explained by different spectral characteristics of the incident radiation at different times of the day, by position of the underwater sensor at different locations under the ice, or partly by experimental error.

## 5. SUMMARY AND CONCLUSIONS

Sixteen days of measurements of incident and under-ice radiation in the 400-700 nm range provides new information in a field where data is severely lacking. The transmittance of photosynthetically active radiation was examined through clear, refrozen slush, and brash ice. Characteristics of the instruments were determined by manufacturers' tests, and support systems for under-ice work were specifically fabricated for this study.

As expected, snow cover played a most important role in radiation diminution. In one data set, transmittance values (ratio of under-ice to incident radiation) of a partially snow-covered, clear ice surface dropped from about 0.80 in a snow-free area to about 0.10 in an area covered by 3 cm of wind-packed snow. An increase in radiation transmittance due to melting snow on an ice surface was also noted. Diffuse extinction coefficients computed for combinations of clear ice, refrozen slush, and varying amounts of snow emphasized the effects of snow cover. In general, ice with thicker snow covers showed higher diffuse extinction coefficients without significant regard to the relative amounts of total ice and refrozen slush.

A relationship between solar altitudes and radiation transmittance was found, under certain circumstances, for refrozen slush. The diurnal dependence of radiation transmittance on solar altitudes is not completely understood, but it is believed that the spectral reflectance characteristics of the ice surface, acting in combination with the diffuse-direct radiation balance, plays an important role. Shading effects due to irregularities in the ice surface are also important. Shading effects of snow banks in artificially cleared areas were also noted.

Changes in cloud cover significantly influenced radiation transmittance when total sky cover changed from clear to cloudy. Variations in transmittance of nearly 20 percent were observed on one occasion.

Varying visual appearance of the ice surface did not necessarily indicate significant changes in radiation transmittance. On one occasion, measurements from the same borehole, under differently appearing ice surfaces, showed a radiation transmittance variation of only 5 percent.

Measurements on brash ice 56 cm thick showed extremely low transmittance with only about 6-7 percent of the radiation reaching the ice-water interface. Considerable snow lodged between the individual ice plates accounted for part of the low transmittance values. Measurements through brash ice before snow accumulates would be valuable.

Surfaces disturbed by snowmobiles showed little difference in radiation transmittance from nearby undisturbed ice-snow combinations. It is felt, however, that this observation is based on site-specific data. Diffuse extinction coefficients for areas disturbed by snowmobiles varied from 0.041 to 0.067.

Diffused extinction coefficients for all ice areas other than snowmobile areas varied from 0.006 for clear ice and a clear-refrozen slush combination during decay to 0.059 for a combination of snow, refrozen slush, and clear ice. Ice surfaces without appreciable snow accumulation showed diffuse extinction coefficients ranging from 0.006 to 0.027.

Results of calculations from a simple two-layer model illustrate the interaction between the various layers of a snow-ice combination. The model shows that even a thin snow cover overlying an ice layer exerts a profound effect on the overall transmittance and reflectance of the combination and this was verified by the field data. The model also shows that ice layers with high reflectance exert some influence on the overall transmittance and reflectance if the upper layer (of snow, frost, etc.) has both reasonably low reflectance and high transmittance.

Irradiance at various water depths below the ice cover was measured and several profiles of ratios of under-ice to incident radiation versus depth from selected dates are included in this report. The measurement of water depth below the ice surface was crude and additional data are required to supplement these data before conclusions are forthcoming.

The data from this study provide considerable additional information to the field of radiation transmittance through ice in the photosynthetically active range. It is also clear that much additional work is required before radiation transmittance in this range is adequately understood. Nevertheless, it should be possible with certain remote sensing systems capable of identifying ice types, either singly or in combination, to provide an assessment of items such as current or predicted winterkill and compensation depth of an ice cover.

## 6. ACKNOWLEDGMENTS

The author would like to express his gratitude to Professors S. I. Outcalt and G. H. Suits of The University of Michigan for their suggestions and advice. Professor Suits is responsible for development of the two-layer model. The assistance of Mr. David Norton of the Great Lakes Environmental Research Laboratory (GLERL) in data collection and computer

programming is gratefully acknowledged. Mr. Frank Rodante of GLERL provided guidance on computer programming. Dr. F. H. Quinn provided technical advice. Mrs. Barbara Lawton and Ms. Pat Willis typed the manuscript.

## 7. REFERENCES

- Anderson, R. S. (1970): Physical Chemical Limnology of Two Mountain Lakes in Banff National Park, Alberta. *J. Fish. Res. Board of Canada*, 27:233-249.
- Bolsenga, S. J. (1977): Preliminary Observations on the Daily Variation Of Ice Albedo. *J. of Glaciol.*, 18:517-521.
- Bolsenga, S. J. (1968): Great Lakes Solar Altitude Charts and Tables. U.S. Lake Survey, Research Report 5-4, pp. 2-3.
- Chandler, D. C. (1942): Limnological Studies of Western Lake Erie - II, Light Penetration and Its Relation to Turbidity. *Ecology*, 23: 41-52.
- Coulson, K. L., and D. W. Reynolds (1971): The Spectral Reflectance of Natural Surfaces. *J. of Applied Meteorol.*, 10:1285-1295.
- Croxton, W. C., W. B. Thurman, and T. Shiffer (1937): The Penetration Of Light through Snow and Ice Cover. *Proceedings, Minnesota Academy of Science*, 5:50-53.
- Goldman, C. R., D. T. Mason, and J. E. Hobbie (1967): Two Antarctic Desert Lakes. *Limnol. and Oceanogr.*, 12:295-310.
- Greenbank, J. T. (1945): Limnological Conditions in Ice-Covered Lakes, Especially as Related to Winter-Kill of Fish. *Ecol. Monogr.*, 15:345-392.
- Halsey, T. G. (1968): Autumnal and Over-Winter Limnology of Three Small Eutrophic Lakes with Particular Reference to Experimental Circulation and Trout Mortality. *J. Fish. Res. Board of Canada*, 25:81-99.
- Idso, S. B., and R. J. Reginato (1974): Assessing Soil-Water Status via Albedo Measurement, Hydrology and Water Resources in Arizona and the Southwest. Proceedings of the 1974 Meetings of the Arizona Section-American Water Resources Association and Hydrology Section - Arizona Academy of Sciences, 4:41-54.
- Idso, S. B., R. D. Jackson, R. J. Reginato, B. A. Kimball, and F. S. Nakayama (1975): The Dependence of Bare Soil Albedo on Soil Water Content. *J. of Applied Meteorol.*, 14:109-113.

- Maguire, R. J. (1975a): Effects of Ice and Snow Cover on Transmission of Light in Lakes. Inland Waters Directorate, Canada Centre for Inland Waters, *Technical Bulletin* No. 54, p. 6.
- Maguire, R. J. (1975b): Light Transmission through Snow and Ice. Inland Waters Directorate, Canada Centre for Inland Waters, *Technical Bulletin* No. 91, p. 4.
- Roemer, S. C., and K. D. Hoagland (1977): Immersion Effect and Cosine Collecting Properties of Li-Cor Underwater Sensors. (Study Conducted for Lambda Instruments Corporation by the School of Life Sciences, University of Nebraska), 1-11.
- Saijo, Y., and M. Sakamoto (1964): Photosynthetic Production of Phytoplankton in Some Ice-Covered Lakes in Central Japan. Recent Researches in the Fields of Hydrosphere, Atmosphere, and Nuclear Geochemistry, 289-303.
- Sauberer, F. (1938): Versuche über Messungen der Stahlungseigenschaften von Schnee und Eis mit Photoelementen. *Meteorol. Zeitschrift*, Band 55, 7:250-255.
- Schindler, D. W., and J. E. Nighswander (1970): Nutrient Supply and Primary Production in Clear Lake, Eastern Ontario. *J. Fish. Res. Board of Canada*, 27:2009-2036.
- Schindler, D. W., et al. (1974): Physical and Chemical Limnology of Char Lake, Cornwallis Island (75°N Latitude). *J. Fish. Res. Board of Canada*, 31:585-607.
- Smith, R. C. (1969): An Underwater Special Irradiance Collector. *J. Mar. Res.*, 27:341-351.
- Tyler, J. E., and R. C. Smith (1970): Measurements of Spectral Irradiance Underwater. New York, New York, Gordon and Breach, p. 103.
- Wright, R. T. (1964): Dynamics of a Phytoplankton Community in an Ice-Covered Lake. *Limnol. and Oceanogr.*, 9:163-178.
- Zinn, D. J., and J. D. Ifft (1941): A New Limnophotometer with a Special Adaptation for the Measurement of the Penetration of Light Through Ice Under Natural Conditions. *Ecology*, 22:209-211.

Appendix. THE TWO-LAYER MODEL

For a two-flow argument (Fig. A.1), the irradiance,  $E(0)$ , is partially reflected from the surface to yield an exitance,  $M(0)$ . The fraction of  $E(0)$  transmitted through layer A yields a portion of  $E(-1)$  which is then reflected from layer B to yield  $E(+1)$ .  $E(+1)$  in turn contributes to  $E(-1)$  and to "stray" radiation reflecting backward and forward in Region 1. The under-ice exitance,  $M(2)$ , represents that portion of  $E(-1)$  transmitted through layer B and radiation in the water that is reflected from the underside of the surface of **layer B from** irradiance  $E(+2)$ . Measurements of  $E(0)$  and  $M(2)$  were made in this study.

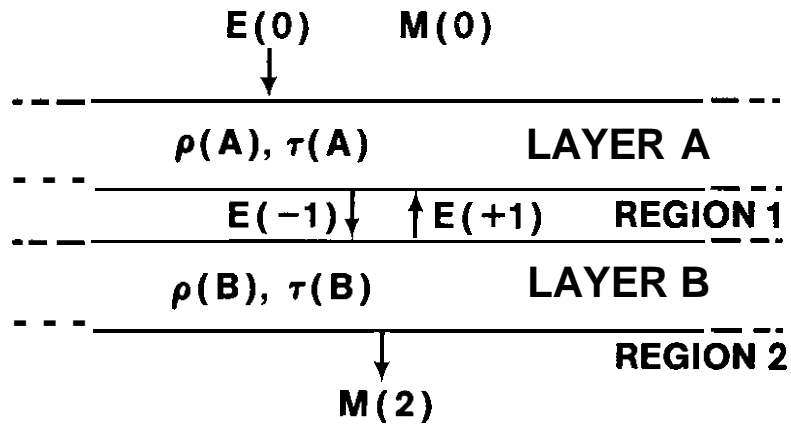


Figure A.1. Schematic representation of two-layer model.

Mathematically, the two-layer model can be expressed:

$$M(0) = E(0)\rho(A) + E(+1)\tau(A) \quad (1)$$

$$E(-1) = E(0)\tau(A) + E(+1)\rho(A) \quad (2)$$

$$E(+1) = \rho(B)E(-1) \quad (3)$$

$$M(2) = \tau(B)E(-1), \quad (4)$$

where

$\rho$  = reflectance,

$\tau$  = transmittance,

A = upper layer,

B = lower layer.

Then,

$$\rho(\text{combination}) = \frac{M(0)}{E(0)} \quad (5)$$

$$\tau(\text{combination}) = \frac{M(2)}{E(0)} \quad (6)$$

$$\rho(C) = \rho(A) + \frac{\tau^2(A)\rho(B)}{1 - \rho(A)\rho(B)} \quad (7)$$

$$\tau(C) = \frac{\tau(A)\tau(B)}{1 - \rho(A)\rho(B)} \cdot \quad (8)$$